HHS Public Access

Author manuscript

Pharmacol Res. Author manuscript; available in PMC 2024 February 01.

Published in final edited form as:

Pharmacol Res. ; 188: 106675. doi:10.1016/j.phrs.2023.106675.

Galanin receptor 3 - a new pharmacological target in retina degeneration

Joseph T. Ortega[1], **Tanu Parmar**[1], **Beata Jastrzebska**[1,#]

[1]Department of Pharmacology and Cleveland Center for Membrane and Structural Biology, School of Medicine, Case Western Reserve University, 10900 Euclid Ave., Cleveland, OH 44106, USA

Abstract

The neuropeptide galanin receptor 3 (GALR3) is a class A G protein-coupled receptor (GPCR) broadly expressed in the nervous system, including the retina. GALR3 is involved in the modulation of immune and inflammatory responses. Tight control of these processes is critical for maintaining homeostasis in the retina and is required to sustain vision. Here, we investigated the role of GALR3 in retina pathologies triggered by bright light and P23H mutation in the rhodopsin (*RHO*) gene, associated with the activation of oxidative stress and inflammatory responses. We used a multiphase approach involving pharmacological inhibition of GALR3 with its antagonist SNAP-37889 and genetic depletion of GALR3 to modulate the GALR3 signaling. Our *in vitro* experiments in the retinal pigment epithelium-derived cells (ARPE19) susceptible to all-*trans*-retinal toxicity indicated that GALR3 could be involved in the cellular stress response to this phototoxic product. Indeed, blocking the GALR3 signaling in $Abca4^{-/-}Rdh8^{-/-}$ and wild-type Balb/cJ mice, sensitive to bright light-induced retina damage, protected retina health in these mice exposed to light. The retina morphology and function were substantially improved, and stress response processes were reduced in these mouse models compared to the controls. Furthermore, in P23H Rho *knock-in* mice, a model of retinitis pigmentosa (RP), both pharmacological inhibition and genetic ablation of GALR3 prolonged the survival of photoreceptors. These results indicate that GALR3 signaling contributes to acute light-induced and chronic RP-linked retinopathies.

[#]**CORRESPONDENCE** Beata Jastrzebska, Ph.D., Department of Pharmacology, School of Medicine, Case Western Reserve University, 10900 Euclid Ave., Cleveland, OH 44106-4965, USA; Phone: 216-368-5683; Fax: 216-368-1300; bxj27@case.edu.

Author's Contributions

B.J., J.T.O., and T.P. conceived the experiments. B.J. and J.T.O. designed the experiments. T.P. conducted initial experiments. J.T.O. and B.J. conducted the experiments that are presented in this manuscript. B.J. and J.T.O. wrote the manuscript. B.J. coordinated and oversaw the project. All authors discussed and commented on the manuscript.

Author Credit Statement

Joseph T. Ortega: Conceptualization, Methodology, Conducting Experiments, Software, Writing-Reviewing and Editing

Tanu Parmar: Methodology, Conducting Experiments, Reviewing

Beata Jastrzebska: Supervision, Conceptualization, Conducting Experiments, Writing- Reviewing and Editing

Declaration of interests

The authors declare that they have no known competing financial interests or personal relationships that could have appeared to influence the work reported in this paper.

CONFLICTS OF INTEREST

The authors declare that they have no conflicts of interest with the contents of this article.

Together, this work provides the pharmacological knowledge base to evaluate GALR3 as a potential target for developing novel therapies to combat retinal degeneration.

Graphical Abstract

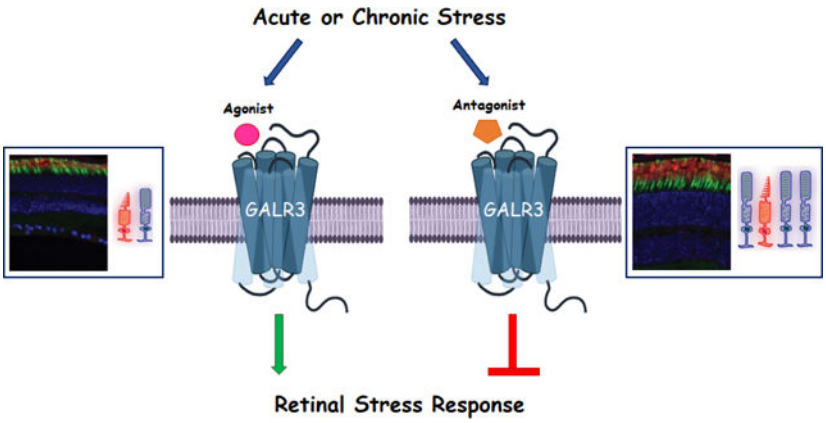

Keywords

galanin receptors; neuroinflammation; photoreceptor; retinal degeneration

INTRODUCTION

The galanin receptors (GALRs), belonging to the family A G protein-coupled receptors (GPCRs), comprise three subtypes GALR1, GALR2, and GALR3 [1, 2]. GALRs are widely distributed in the nervous system but are also expressed in non-neuronal tissues [2, 3]. These receptors have high sequence homology and structural similarity. However, their tissue distribution pattern and type of G protein through which they signal differ. While GALR1 and GALR3 predominantly couple to $G_{i/o}$, with consequent reduction of cAMP and inactivation of protein kinase A, GALR2 signals preferentially via G_q, resulting in the activation of protein kinase C [1]. Two major endogenous ligands of GALRs, galanin and spexin show cross-reactivity to all three receptor subtypes. However, spexin preferentially activates GALR2 and GALR3, whereas galanin has a high affinity for GALR1 and GALR2, but not GALR3 [2, 4]. GALRs signaling plays a pivotal role in modulating homeostasis of various physiological processes, such as metabolism, nociception, cognition, feeding behavior, and inflammatory response [5, 6]. Importantly, GALR3-mediated signaling plays a central role in the pathogenesis of many human diseases, including epilepsy, alcoholism, neuropathic pain, diabetes, and cancer for which the activation of inflammatory response is a major hallmark [6–10]. In addition, GALR3 is involved in the regulation of inflammatory processes occurring in progressive degenerative diseases such as arthritis, psoriasis, and pancreatitis, and in neurodegeneration, including Alzheimer's disease [11–15]. Interestingly, a blood-brain barrier permeable and highly selective small molecule antagonist of GALR3, namely SNAP-37899 administered to murine models of stress, depression, and alcohol abuse resulted in the diminishing of these CNS-related disorders [12, 16–18].

Galanin receptors could also play an important role in ocular homeostasis [19, 20]. The retinal function requires a controlled supply of oxygen and nutrients together with timely removal of toxic metabolites in a tightly regulated environment provided by the cellular blood-retina barrier [21]. These processes are rigorously controlled by multiple mechanisms, including GPCR signaling [19, 22–25]. Interestingly, the endogenous GALR agonists and their receptors GALR1-3 are expressed in the human retina [19, 26, 27]. Among the three GALRs, GALR3 is specifically abundant in the retinal pigment epithelium (RPE) cells and around choroidal vessels, tissues important for the retina supply and its detoxification from byproducts generated by light. In addition, GALR3 was found on the surface of immune cells such as microglia and neutrophils that are involved in maintaining retinal homeostasis, thus modulation of GALR3 signaling could have significant implications in retinal pathologies [28, 29]. A disruption in retinal homeostasis often leads to retinal degenerative diseases [30]. Accumulated evidence indicates that modulation of the GPCR signaling provides neuroprotective effects, preventing degeneration in mouse models of retinopathy [31, 32]. However, the exact mechanism of protection through the GPCR-mediated modulators is unclear and only a handful of GPCRs have been targeted therapeutically. Indeed, modulators of GPCRs, adenylate cyclase (AC), phospholipase C (PLC), and Ca^{2+} channel blockers can mitigate pathological development in the *Abca4*$^{-/-}$*Rdh8*$^{-/-}$ mice, a model of human Stargardt diseases and age-related macular degeneration (AMD), emphasizing the role of GPCRs in the development and progression of retinal degeneration [33, 34]. Pathogenesis of degenerative retinal diseases is associated with chronic inflammatory responses occurring in retinal cells [35–37]. In degenerating retinas of *Abca4*$^{-/-}$*Rdh8*$^{-/-}$ the inflammatory mechanisms are triggered by high levels of toxic photoproducts, including all-*trans*-retinal and its conjugates [33, 34]. Activation of the inflammatory-stress signaling pathway is also a hallmark of retinitis pigmentosa (RP). This retinopathy is triggered by mutations in multiple retina-specific genes, including rod visual receptor, rhodopsin (Rho). The most common Pro 23 to His substitution in Rho accounts for 10–12% of all autosomal dominant RP (adRP) cases, without a therapeutic option available [38–40]. Interestingly, GALR3-mediated signaling is involved in the regulation of the inflammatory process associated with progressive irreversible degeneration [11–15].

The complexity of the GALRs-mediated signal transduction systems and tissue response emphasizes the need for a better understanding of the pathophysiological functions of these receptors. In this study, we aimed to investigate the role of GALR3 in retina degeneration. By applying the pharmacological GALR3 inhibition with its selective SNAP-37889 antagonist [16] and genetic ablation of GALR3 in mouse models of acute and chronic retina degeneration, we found that GALR3 signaling contributes to pathologies of both, light-induced and P23H Rho-linked RP retinopathies [41]. Blocking GALR3 signaling showed protective effects against light-stimulated retina damage in *Abca4*$^{-/-}$*Rdh8*$^{-/-}$ and WT Balb/cJ mice and prolonged survival of photoreceptors in a mouse model of RP associated with Rho misfolding. These results suggest the potential of GALR3 as a new target for developing therapies against these retinopathies.

MATERIAL AND METHODS

Chemicals and Reagents

Dimethylsulfoxide (DMSO) and EDTA-free protease inhibitor cocktail tablets were purchased from Sigma (St. Louis, MO). Peanut agglutinin (PNA) and Alexa Fluor 488-conjugated streptavidin were purchased from Vector. 4969-Diamidino-2-phenyl-indole (DAPI) for the nuclear staining was purchased from Life Technologies (Grand Island, NY). Polyvinylidene difluoride (PVDF) membrane was obtained from Millipore (Burlington, MA). The GALR3 inhibitor SNAP-37889 was purchased from Alomone Labs (Jerusalem, Israel) (PubChem CID 1471834). The GALR3 activator galnon was purchased from Sigma (PubChem CID: 5311268). pCMV6-GALR3-(Myc-DDK-tagged) DNA was purchased from OriGene Technologies (Rockville, MD). Polyethylenimine was obtained from Sigma. 3-(4,5-dimethylthiazol-2-yl)-2,5-diphenyltetrazolium bromide (MTT) was also purchased from Sigma. All the antibodies used in this study are listed in Table 1.

Animals Care

Abca4$^{-/-}$*Rdh8*$^{-/-}$ mice were used to examine the effects of GALR3 inhibitor SNAP-37889 against light-induced retinal degeneration. These mice were free of the *Rd8* mutation and they had the Leu variation at amino acid 450 of the retinal pigment epithelium 65 kDa protein gene (*Rpe65*), which increases sensitivity to bright light [42, 43]. Mice with Met variation exhibit decreased sensitivity to bright light [42]. *Galr3*$^{-/-}$ mice (**RRID**:IMSR_TAC:tf0230) (Taconic, Germantown, NY) were used to evaluate GALR3 as a pharmacological target. *Galr3*$^{-/-}$ mice are on C57BL/6J background, thus C57BL/6J mice (**RRID**:IMSR_JAX:000664) (Jackson Laboratory, Bar Harbor, ME) were used as wild-type (WT) control. *Galr3*$^{-/-}$ mice were crossed with Balb/cJ mice (**RRID**:IMSR_JAX:000651) to generate light-sensitive *Galr3*$^{-/-}$ mice. These mice were used to evaluate the effect of *Galr3* gene depletion on acute retinal degeneration caused by bright light insult. Balb/cJ mice were used as WT control. Heterozygous *Rho*$^{P23H/+}$ *knock-in* mice were crossed with *Galr3*$^{-/-}$ mice to examine if lack of GALR3 has a beneficial effect on chronic retinopathy caused by P23H mutation in *Rho* gene. *Rho*$^{P23H/P23H}$ (Research Resource Identifier, **RRID**:IMSR_JAX:017628) were crossed with C57BL/6J mice (**RRID**:IMSR_JAX:000664), (Jackson Laboratory, Bar Harbor, ME) to obtain heterozygous *Rho*$^{P23H/+}$ mice. Both male and female mice were used in all experiments. All mice were housed in the Animal Resource Center at the School of Medicine, Case Western Reserve University (CWRU), and maintained in a 12-hour light/dark cycle. All the procedures involving mice and experimental protocols were approved by the Institutional Animal Care and Use Committee at CWRU and conformed to recommendations of both the American Veterinary Medical Association Panel on Euthanasia and the Association for Research in Vision and Ophthalmology as well as the National Eye Institute Animal Care and Use Committee (NEI-ASP 682). Efforts were taken to minimize animal suffering.

Light-Induced Retinal Degeneration and Treatment Conditions

Abca4$^{-/-}$*Rdh8*$^{-/-}$ mice at six weeks of age, Balb/cJ mice at eight weeks of age, and *Galr3*$^{-/-}$ mice at eight weeks of age on Balb/cJ background were dark-adapted 24 h before the treatment. The GALR3-specific inhibitor, SNAP-37889 [16], was dissolved in 50%

DMSO in phosphate-buffered saline (PBS) and delivered to mice via intraperitoneal (i.p.) injection. SNAP-37889 at a concentration of 100 mg/kg body weight (b.w.) or vehicle were administered to mice 30 min before exposure to bright light (Screw-In compact fluorescent (CFL) Bulb: spiral, 42 Watt bulb equivalent to 150 Watt incandescent bulb (soft white with brightness of 2,850 lumens, and minimum starting temperature of −28.9 °C), Grainger. *Abca4*$^{-/-}$*Rdh8*$^{-/-}$ mice were exposed to 10,000 lux light for 30 min, while Balb/cJ and *Galr3*$^{-/-}$ mice were exposed to 12,000 lux light for 1 h [43, 44]. The light exposure was performed between 9.00 and 10.00 am. Pupils of these mice were dilated with 1% tropicamide prior to light exposure. After illumination, mice were maintained in the dark for 7 days and then analyzed. Retinal morphology was visualized *in vivo* by spectral domain-optical coherence tomography (SD-OCT) (n = 6 mice per group) and scanning laser ophthalmoscopy (SLO) (n = 6 mice per group). Electroretinography (ERG) was used to assess retinal function (n = 5 mice per group). Before each procedure, mice were anesthetized with a cocktail composed of ketamine (20 mg/ml) and xylazine (1.75 mg/ml) at a dose of 4 μl/g b.w. Mice were euthanized by cervical dislocation under deep anesthesia before the collection of eyes. For histological evaluation, eyes (n = 6 mice per group) were fixed in either 4% formalin in PBS or 2% glutaraldehyde followed by 2% paraformaldehyde. These eyes were embedded in paraffin and sections were stained with hematoxylin and eosin (H&E).

Treatment of *Rho*$^{P23H/+}$ Mice

The effect of the inhibition of GALR3 with its specific inhibitor SNAP-37889 [16] on the progression of retinal degeneration in RP was examined in *Rho*$^{P23H/+}$ mice [45]. SNAP-37889 at 10 mg/kg b.w. or vehicle was administered i.p. to mice every other day at 3.00 pm. Six injections total were performed. Mice were examined at postnatal day 33 (P33) as described in [46]. The changes in retinal morphology upon drug treatment were assessed with SD-OCT (n = 6 mice per group) and retinal function was examined with ERG (n = 5 mice per group). Before each procedure, mice were anesthetized with a cocktail containing ketamine (20 mg/ml) and xylazine (1.75 mg/ml) at a dose of 4 μl/g b.w. For histological retina evaluation and immunohistochemistry, mice were euthanized by cervical dislocation under deep anesthesia before eyes collection (n = 6 per group).

In vivo Retina Imaging

To examine the effect of pharmacological inhibition and genetic depletion of GALR3 on acute retinal degeneration induced by bright light retina or chronic degeneration caused by P23H mutation in Rho, the retina was imaged *in vivo* using the ultrahigh-resolution Spectral-Domain Optical Coherence Tomography (SD-OCT) (Bioptigen, Morrisville, NC). The a-scan/b-scan ratio was set at 1200 lines. The OCT images were obtained by scanning at 0 and 90 degrees in the b-mode. Five image frames were captured and averaged. Changes in the retina of treated and control mice were determined by measuring the thickness of the outer nuclear layer (ONL) at 0.5 mm from the optic nerve head (ONH). The following mouse strains were subjected to SD-OCT imaging: *Abca4*$^{-/-}$*Rdh8*$^{-/-}$, Balb/cJ, C57BL/6J, *Galr3*$^{-/-}$ on either C57BL/6J or Balb/cJ background, *Rho*$^{P23H/+}$, *Galr3*$^{-/-}$*Rho*$^{P23H/+}$. Six mice were used in each experimental group.

The *in vivo* whole-fundus imaging of the mouse retina was performed with the Scanning Laser Ophthalmoscopy (SLO) (Heidelberg Engineering, Franklin, MA) immediately after the SD-OCT imaging. The auto-fluorescence mode was used. The number of autofluorescent spots (AF) detected in different experimental groups was quantified and compared between the experimental groups to determine the statistical significance. The following mouse strains were subjected to SD-OCT imaging: $Abca4^{-/-}Rdh8^{-/-}$, $Galr3^{-/-}$ on Balb/cJ background, and Balb/cJ. Six mice were used in each experimental group.

Retinal Histology

Mouse eyes (n = 6 per group) were collected from euthanized mice and fixed in 0.5% glutaraldehyde in 2% paraformaldehyde (PFA) in PBS for 24 h at RT on a rocking platform followed by their incubation in 1% PFA for 48 h at RT. These eyes were embedded in paraffin and sectioned. Sections (5 μm thick) were stained with hematoxylin and eosin (H&E). The retina imaging was performed with a ZEISS Axio Scan.Z1 slide scanner (Carl Zeiss Microscopy GmBH, Jena, Germany) and analyzed using Zeiss-Zen 3.2 software (blue edition).

Immunohistochemistry

To detect rod and cone photoreceptors in the retina, eyes were collected from the following groups of mice: (1) dark-adapted, and vehicle or SNAP-37889-treated, exposed to bright light $Abca4^{-/-}Rdh8^{-/-}$, and Balb/cJ WT mice, (2) $Galr3^{-/-}$ on Balb/cJ background mice, which were either dark-adapted or exposed to bright light, (3) C57BL/6J WT and $Galr3^{-/-}$ on C57BL/6J background mice (2, 4 and 8-months-old), and (4) $Galr3^{-/-}Rho^{P23H/+}$ and $Rho^{P23H/+}$ mice at P33. Eyes were fixed in 4% PFA for 24 h followed by their incubation in 1% PFA for 48 h at RT. Cryosections, 8 μm thick, prepared from fixed eyes were blocked with 10% normal goat serum (NGS) and 0.3% Triton X-100 in PBS for 1 h at RT and then stained overnight at 4°C with a monoclonal mouse 1D4 anti-Rho primary antibody to visualize rod photoreceptors and biotinylated peanut agglutinin (PNA) (1:500 dilution) to visualize cone photoreceptors. The next day, sections were washed with PBS, followed by the 2 h incubation with the secondary antibody at RT, Alexa Fluor 555-conjugated goat anti-mouse secondary antibody (1:400 dilution) to detect rods and Fluor 488-conjugated streptavidin (1:500 dilution) to detect cones. To determine the localization of GALR3 in the mouse retina, the retina sections were stained with a rabbit polyclonal anti-GALR3 antibody recognizing the extracellular motif (1:200 dilution). The expression level of GFAP was detected with a rabbit polyclonal anti-GFAP antibody (1:1000). Cell nuclei were detected by staining with DAPI. Slides were coverslipped with Fluoromount-G (SouthernBiotech).

ERG

To examine the effect of the genotype and SNAP-37889 treatment on retinal function electroretinography (ERG) was performed. Scotopic and photopic ERGs were recorded for both eyes of each mouse using a Celeris rodent ERG system and Espion Dyagnosys software Version 6 (Dyagnosys, LLC, Lowell, MA). The ERG data were processed for each experimental group and presented as mean and standard deviation (S.D.) for both a-wave and b-wave amplitudes. Each experimental group contained n = 5 mice.

Purification of Rho

Mouse eyes, collected under dim red light (n = 6) per group were gently homogenized in a glass-glass homogenizer in 2 ml of 20 mM Bis-tris propane (BTP), 120 mM NaCl, 1 mM EDTA, and protease inhibitor cocktail, pH 7.5, followed by centrifugation at 16,000*g* for 10 min at 4 °C. The supernatants were discarded, while pellets were incubated in 20 mM BTP, 120 mM NaCl, 20 mM n-dodecyl-β-D-maltopyranoside (DDM), and protease inhibitor cocktail, pH 7.5 for 1 h at 4 °C on nutator to solubilize the membranes. The lysates were centrifuged at 100,000*g* for 1 h at 4 °C and Rho was purified from the supernatant by immunoaffinity chromatography with an anti-Rho C-terminal 1D4 antibody immobilized on CNBr-activated agarose. Three hundred μl of 6 mg 1D4/ml agarose beads were added to the supernatant and incubated for 1 h at 4 °C on the nutator. The resin was then transferred to a column and washed with 15 ml of 20 mM BTP, 120 mM NaCl, and 2 mM DDM, pH 7.5. Rho was eluted with the same buffer, supplemented with 0.6 mg/ml of the TETSQVAPA peptide. The UV-visible spectra of freshly purified Rho samples were measured in the dark with a UV-visible spectrophotometer (Cary 60, Varian, Palo Alto, CA).

Retinoid Analysis

Retinoids were extracted from mouse eyes (n = 5 mice/ group) collected under dim red light by using the established procedures [47]. Briefly, eyes were homogenized in methanol/PBS (50/50 volume/volume) solution, containing hydroxylamine (pH 7.5) added to 40 mM final concentration, followed by 20 min incubation at RT. The obtained retinal oximes were extracted with hexane and their isomeric content was determined by normal phase high-performance liquid chromatography (HPLC) with a Luna 10 μm PRE-Silica 100 Å, 250 × 4.6 mm column (Beckman, San Ramon, CA) (3). Retinoids were eluted isocratically with 10% ethyl acetate in hexane at a flow rate of 1.4 ml/min. Their signals were detected by absorption at 360 nm [48].

Immunoblotting

The proteins were extracted from the whole mouse eyes. Five mice per treatment group were used. The eyes were mechanically homogenized in an NP40 lysis buffer (Invitrogen) containing a protease inhibitor cocktail (Roche) followed by 30 min incubation at 4 °C. The lysates were centrifuged at 12,000*g* for 15 min at 4 °C. The protein concentration was measured with a BCA Protein Assay Kit (Thermo Fisher Scientific) with bovine serum albumin as a standard. The protein extract (50 μg/lane) was mixed with a sample buffer and loaded on an SDS-PAGE gel. The protein samples were separated with 10% SDS-PAGE gel electrophoresis and then transferred to a polyvinylidene difluoride (PVDF) membrane (Millipore). The PVDF membrane was incubated with the primary antibodies followed by horseradish peroxidase (HRP)-conjugated anti-mouse or anti-rabbit secondary antibody listed in Table 1. The immunoblots were developed with a ProSignal reagents kit and the Odyssey Imaging System (LI-COR, Biosciences). GAPDH was used as the loading control.

Cell Culture

The ATCC ARPE19 and HEK-293T cells were cultured in Dulbecco’s Modified Eagle Medium (DMEM) with 10% fetal bovine serum (FBS) (Hyclone, Logan, UT), and 1 unit/ml

penicillin with 1 μg/ml streptomycin (Life Technologies) at 37 °C under 5% CO_2 according to the instructions from the ATCC Animal Cell Culture Guide. The experiments were conducted within cell passages of 10–15.

Transfection

The HEK-293T cells were plated into a 10 cm diameter plate. The next day, at ~80% confluency, these cells were transiently transfected with mouse pCMV6-GALR3-(Myc-DDK-tagged) constructs (OriGene Technologies, Rockville, MD) using polyethyleneimine [49, 50]. Forty eight hours after transfection cells were collected and immediately used for protein extract preparation or the cell pellet was kept at − 80 °C.

Cell Viability Assay

The ARPE19 cells were seeded in a 96-well plate at a density of 30,000 cells/ well in 85 μl of DMEM medium containing 10% FBS and antibiotics. Sixteen hours later different concentrations of SNAP-37889 (0.0001 – 1 μM) or all-*trans*-retinal (0.3 – 30 μM) were added to the cells for 1 h or 24 h. Alternatively, cells were treated with 0.5 μM SNAP-37889 for 30 min followed by galnon stimulation (0.05 μM for 30 min), and later the addition of all-*trans*-retinal at 10 or 30 μM for either 1 or 24 h. The effect of galnon (0.0001 – 1 μM) on cell viability was also examined. The cell viability was examined with the MTT proliferation assay (Sigma) [51]. The percentage of viable cells under these conditions was calculated.

cAMP Detection Assay

The ARPE19 cells were plated in two 96-well plates at a density of 50,000 cells/ well in 85 μl of DMEM medium containing 10% FBS and antibiotics. Sixteen hours after seeding the cells were treated with SNAP-37889 at 10 μM concentrations for 30 min. Next, galnon at 0.001, 0.1, or 1 μM was added for 30 min. Levels of accumulated cAMP were detected with the cAMP-Glo™ kit (Promega) following the manufacturer's protocol. The luminescence signal was recorded with a FlexStation 3 plate reader (Molecular Devices). The cAMP provided by the kit was used to prepare the standard curve. The percentage of cAMP was calculated for each condition, assuming the cAMP level detected in the non-treated cells as 100%. Each condition was performed in triplicate and the experiment was repeated.

Cell Death Detection

To quantify the apoptotic retinal cells the **T**dT-mediated d-**U**TP-X **n**ick **e**nd **l**abeling (TUNEL) was performed using *in situ* death detection kit (Roche) according to the manufacturer's protocol. The retinal cryosections (8 μm thick) were incubated in PBS with 1% Triton X-100 (v/v) for 8 min at RT followed by the incubation with TUNEL mix reagent for 1 h at °C in the humidity chamber in the dark. Then, the slides were washed 4 times with PBS, mounted in Fluoromount-G, coverslipped, and imaged.

RT-qPCR

The selected gene expression analysis was carried out in mouse eyes collected from n = 5 mice per treatment group. RNA isolation was obtained from the whole eye extracts by using the Qiagen RNeasy Miniprep Kit following the manufacturer's protocol. Then,

the samples were treated with DNase I and RNA concentration was determined using a nanodrop spectrophotometer (Thermo Fisher Scientific). The RNA served as a template to obtain cDNA by using the QuantiTect Reverse Transcription Kit (Qiagen) following the manufacturer's protocol. Quantitative RT-PCR amplification was performed using LUNA NEB SYBR Green Master Mix (NEB) using the StepOnePlus Real-Time PCR system (Applied Biosystems). The PCR conditions were as follows: 95°C for 3 min followed by 40 cycles of 95°C for 20 s and 60°C for 60 s. Fluorescence data were acquired at the step of 60°C and a Melt curve step was added. *Gapdh* was used as a control housekeeping gene. All data were normalized to the *Gapdh* expression level, and the fold change was calculated for each gene. The C_t values were obtained from the amplification curve analysis using StepOne software version 2.3. The gene expression was measured using the comparative $2^{-(\Delta\Delta Ct)}$ method. All primers used in this study are listed in Table 2.

Statistical Analyses

The detection of cAMP levels was performed in triplicates and repeated two times. Immunoblots were performed 3 times and protein bands were quantified using ImageJ software. Each assay included positive and negative controls. The data obtained from these analyses were shown as an average and standard deviation (S.D). For multiple comparisons, one or two-way ANOVA with Turkey's post hoc tests were used. All statistical calculations were performed using the Prism GraphPad 7.02 software. Type 1 error tolerance for the experiments was established at 5%. Values of $P < 0.05$ were considered statistically significant. Distinct personnel carried out the collection of data and its statistical analysis.

RESULTS

Inhibition of GALR3 signaling negatively modulates all-*trans*-retinal toxicity.

Aberrant metabolism of all-*trans*-retinal and its byproducts is a hallmark of retina degeneration associated with aging and Stargardt disease [33, 34, 52, 53]. RPE cells are especially vulnerable to the toxicity of retinoid byproducts [53–55]. Modulation of GPCR signaling can lessen all-*trans*-retinal toxicity and alleviate retina degeneration [31]. To inspect if GALR3-mediated signaling plays a role in all-*trans*-retinal toxicity and if its modulation can mitigate or delay retina degeneration, we first used a simplified system of the RPE-derived human ARPE19 cells to assess the expression of GALRs in this model. We found that the ARPE19 cells express GALR3 along with GALR2, but GALR1 was not detected (Fig. 1A). The GALRs signaling was evidenced by a decrease in the cAMP cellular pool after the stimulation with a small molecule agonist of GALRs, galnon, in a dose-response fashion (Fig. 1B). To modulate the GALR3 response, we employed a well-known GALR3-specific antagonist, SNAP-37889 [16]. Treatment with SNAP-37889 did not affect G_i-related signaling in the ARPE19 cells in the absence of the agonist. However, prior treatment with SNAP-37889 efficiently inhibited signal transduction in cells later stimulated with galnon (Fig. 1B). Moreover, SNAP-37889 or galnon at 0 – 1 μM concentration did not change cell viability up to 24 h incubation (Fig. 1D and Fig. S1).

Next, we examined if modulation of GALR3-mediated signaling with the specific inhibitor of this receptor SNAP-37889 can ameliorate the toxic effects of all-*trans*-retinal. The

exposure of the ARPE19 cells to all-*trans*-retinal (0.3 – 60 μM) evidently decreased the number of viable cells by ~10 to 40% in a concentration-dependent manner detected after 1 h incubation and by ~30 to 80% detected after 24 h incubation with the stressor (Fig. 1C). However, pretreatment of cells with SNAP-37889 at 0.5 and 1 μM before adding all-*trans*-retinal resulted in a substantial enhancement of cell survival (Fig. S2). Treatment of the ARPE19 cells with 0.05 μM galnon agonist prior to all-*trans*-retinal stress slightly exacerbated the all-*trans*-retinal toxicity, while pretreatment with 0.5 μM SNAP-37889 prior to stimulation of GALR3 with galnon resulted in the protection of cells against all-*trans*-retinal toxicity detected 1 h and 24 h after exposure to the stressor (Fig. 1E–F). These results encouraged further study in mice susceptible to bright light-induced retina degeneration to test the effectiveness of inhibition of the GALR3-mediated signaling as a strategy for protecting the health of the retina.

GALR3 is expressed in the mouse retina

The expression of GALR3 in the human eye was reported previously [19]. GALR3 immunoreactivity was found in the choroidal neurons, nerve fibers of the choroidal stroma, the choroidal blood vessels, and choriocapillaris. GALR3 was also present in the inner nuclear layer (INL) and retinal pigment epithelium (RPE) of the human retina. By using immunohistochemistry and mouse eye cryosections, we confirmed that GALR3 is expressed in the neurons located within the INL, in the RPE cells, and the ganglion cells in the retinas of *Abca4*$^{-/-}$*Rdh8*$^{-/-}$ and WT mice (Fig. 1G, Fig. S3, and Fig. S4). *Abca4*$^{-/-}$*Rdh8*$^{-/-}$ mice feature many hallmarks of human Stargardt disease, a juvenile AMD [33, 34]. Due to the ablation of two genes encoding ABCA 4 transporter (*Abca4*) and retinol dehydrogenase 8 (*Rdh8*), which are critical for retinoid homeostasis, these mice develop severe retinal degeneration in response to bright light exposure. Accumulating free all-*trans*-retinal released upon illumination and its byproducts activate inflammatory responses that aggravate degenerative processes in these mice photoreceptors. GALR3 signaling is involved in the modulation of various inflammatory processes, including neuroinflammation. Thus, we sought to examine if inhibition of GALR3 signaling could protect retinas from light-induced retinal degeneration. First, we examined if bright light insult has an effect on the expression of GALR3 in the eyes of *Abca4*$^{-/-}$*Rdh8*$^{-/-}$ mice. Interestingly, the mRNA expression of GALR3 was increased in the eyes of these mice exposed to bright light seven days later by ~4 folds as compared to dark-adapted mice and protein expression increased by ~1.2 fold (Fig. 1H–I). Moreover, the mRNA expression of the endogenous GALR3 agonist, spexin was also elevated on day seven post illumination by ~4 folds. Thus, the exposure of *Abca4*$^{-/-}$*Rdh8*$^{-/-}$ mice to excessive light stimulated changes in the expression of GALR3 suggesting the involvement of the GALR3-mediated signaling in the retina degenerative processes triggered by intense light stress.

Pharmacological inhibition of GALR3 protects the retina of *Abca4*$^{-/-}$*Rdh8*$^{-/-}$ mice from light-induced retina degeneration.

GALR3-mediated signaling is associated with neurodegeneration, including Alzheimer's disease [13]. GALR3 is also involved in the regulation of inflammatory processes associated with progressive degeneration [11, 56]. Inflammation is one of the hallmarks of retina degeneration induced by excessive light in *Abca4*$^{-/-}$*Rdh8*$^{-/-}$ mice [33, 34]. As reported

previously, modulation of the GPCR-mediated signaling in these mice protected retinas from light-induced degeneration. Thus, we sought to investigate if inhibition of GALR3 could serve as a protective mechanism to alleviate degenerative processes triggered by exposure to bright light. *Abca4*$^{-/-}$*Rdh8*$^{-/-}$ mice were administered with either a specific inhibitor of GALR3, SNAP-37889, or vehicle 30 min before illumination, and then exposed to 10,000 lux light for 30 min (Fig. 2A). Control mice were kept in the dark. The analysis of retina morphology seven days later by SD-OCT imaging revealed that as expected photoreceptors in the vehicle-treated mice were severely damaged. However, the retinas of mice treated with the GALR3 inhibitor appeared healthy and closely resembled the retinas of the dark-adapted mice (Fig. 2B–C). Light-induced retinal degeneration is associated with the activation of the immune response. Activated glial cells and the retina infiltrating macrophages can be visualized in the whole fundus with spectral domain ophthalmoscopy (SLO) as autofluorescence (AF) spots. The abundance of AF spots was detected in the retinas of *Abca4*$^{-/-}$*Rdh8*$^{-/-}$ mice injured with light. However, they were not detected in mice pretreated with SNAP-37889 (Fig. 2D–E). The structural organization of the retina was also inspected in the H&E-stained retinal sections and cryosections labeled with 1D4 antibodies recognizing Rho to detect rod photoreceptors and peanut agglutinin to detect cone photoreceptors. Both analyses indicated severe photoreceptor damage in mice treated with the vehicle and illuminated with bright light, while the retinas of mice treated with SNAP-37889 before illumination closely resembled those of unexposed mice (Fig. 2F–G). In addition, retinal function assessed by a recording of the electroretinography (ERG) responses was preserved in mice treated with the GALR3 inhibitor. Both a- and b-wave amplitudes closely resembled the responses of dark-adapted control mice (Fig. 2H). Together, these results indicate the importance of GALR3 signaling in the progression of degenerative processes in the retina associated with intense light exposure.

Pharmacological inhibition of GALR3 protects the retina of WT mice from light-induced retina degeneration.

The effect of GALR3 inhibition with SNAP-37889 on light-induced retina degeneration was also examined in the WT Balb/cJ mice. These albino mice are susceptible to retina damage upon exposure to intense light. We used a similar treatment strategy with SNAP-37889 as developed for *Abca4*$^{-/-}$*Rdh8*$^{-/-}$ mice (Fig. 2A). Seven days after illumination, the retina of the vehicle-treated mice was severely damaged with the ONL layer substantially thinner due to photoreceptors death. However, the retina morphology of SNAP-37889-treated mice prior to light exposure was similar to the dark-adapted mice (Fig. 3A–B and E-F). The number of AF that largely increased in the light-exposed mice, in mice treated with SNAP-37889 before illumination closely resembled the AF number found in unexposed mice (Fig. 3C–D). An inhibition of GALR3 was also advantageous for retinal function as detected in the ERG responses. Both, the scotopic a- and b-waves, and photopic b-waves were substantially improved in mice treated with SNAP-37889 prior to illumination (Fig. 3G). Altogether, our results indicated the beneficial effect of GALR3 inhibition on retinal health counteracting the damaging effects of bright light-induced retina degeneration in both *Abca4*$^{-/-}$*Rdh8*$^{-/-}$ and WT mice.

Genetic ablation of GALR3 prevents light-induced retina damage.

To gain more evidence that GALR3 could be a novel pharmacological target in retinal degenerative diseases, we examined if genetic depletion of *Galr3* could preserve the retina morphology and function under bright light stress. Thus, *Galr3*$^{-/-}$ mice were cross bread with Balb/cJ mice to establish *Galr3*$^{-/-}$ mice susceptible to acute light retina injury (Fig. S5). Six to eight-month-old *Galr3*$^{-/-}$ mice were exposed to bright light along with the WT Balb/cJ mice as a control (Fig. 4 and Fig. 3). While WT mice after seven days from illumination developed severe retina degeneration, the retinas of mice lacking *Galr3* were less sensitive to bright light injury.

The *in vivo* SD-OCT imaging showed that the overall retina morphology and the ONL thickness in *Galr3*$^{-/-}$ illuminated mice were similar to those in unexposed mice (Fig. 4A–B). The increase of AF spots that accumulate upon illumination with excessive light in WT Balb/cJ mice was not detected in *Galr3*$^{-/-}$ mice (Fig. 4C–D). The retina structure examined by H&E staining and immunohistochemical detection of photoreceptors did not reveal major differences between unexposed and illuminated *Galr3*$^{-/-}$ mice (Fig. 4E–F). The ERG responses were slightly lower in *Galr3*$^{-/-}$ mice exposed to bright light insult (Fig. 4G). However, the ERG amplitudes were substantially higher in these mice as compared to WT Balb/cJ mice exposed to light (Fig. 4H). Together, these results indicate that modulation of GALR3 signaling could be advantageous in efforts to develop novel treatments for retinopathies associated with toxicity of bright light.

Inhibition of GALR3 signaling prevents photoreceptor cell death

To confirm the beneficial effects of GALR3 inhibition on retinal health, we examined levels of Rho and M cone opsin in the retinas of WT Balb/cJ mice dark-adapted, exposed to bright light, and treated with SNAP-37889 prior to illumination, as well as unexposed and illuminated *Galr3*$^{-/-}$ mice. Rho is a major structural protein required for the development of rod outer segments (ROS) in the rod photoreceptors and the visual receptor activated by photons. Thus, its unaffected expression is critical for proper retina morphology and rod function. The levels of Rho examined by the immunoaffinity purification confirmed the lesser concentration of this receptor in WT Balb/cJ mice exposed to light stress (Fig. 5A, left panel, and B). However, Rho levels were substantially higher in these mice pretreated with GALR3-specific inhibitor SNAP37889 prior to light injury (Fig. 5A, left panel, and B). In *Galr3*$^{-/-}$ mice, we did not detect any difference in the levels of Rho between illuminated and unexposed mice (Fig. 5A, right panel, and B). In addition, no major differences in Rho levels were found between WT and *Galr3*$^{-/-}$ mice unexposed to light. Similarly, levels of M cone opsin were affected by light exposure in WT Balb/cJ mice, but either pharmacological or genetic depletion of GALR3 signaling resulted in higher M cone opsin levels (Fig. 5C–D and Fig. S6). As inspected by RT-qPCR both pharmacological treatment with GALR3 inhibitor and ablation of *Galr3* gene resulted in stimulation of the expression of Rho and M cone opsin in retinas of mice exposed to light, suggesting that the change in the expression of these key photoreceptor proteins is critical for maintaining retina health under the excessive light stressor (Fig. 5E–F).

Inhibition of GALR3 signaling modulates light-induced inflammatory processes in the retina

Exposure of mice to excessive light leads to the activation of retinal inflammation. Among other factors, this process is associated with the elevation of glial fibrillary acidic protein (GFAP) in the retina. Indeed, an increased level of GFAP was detected in WT Balb/cJ mice injured with bright light. Interestingly, in both WT Balb/cJ mice treated with SNAP-37889 and in *Galr3*$^{-/-}$ mice exposed to light, levels of GFAP were comparable to those detected in unexposed mice (Fig. 6A–C). The inflammatory processes occurring in the retina injured with bright light induced the programmed cell death of photoreceptor cells. Dying photoreceptors were detected in the retinas of light-exposed WT Balb/cJ mice by using the TUNEL staining analysis. Interestingly, treatment with the GALR3 inhibitor SNAP-37889 prior to illumination protected the retina health in these mice (Fig. 6D–E). Similarly, genetic depletion of GALR3 inhibited the apoptotic processes induced by bright light. TUNEL-positive photoreceptor cells were not found in *Galr3*$^{-/-}$ mice exposed to light (Fig. 6D–E). In addition, elevated levels of several apoptosis-associated markers such as interleukin 1-β (IL1-β), interleukin 6 (IL6), chemokine 2 (CCL2), and tumor necrosis factor α (TNF-α) were found in WT Balb/cJ mice exposed to bright light. The expression of these markers was substantially reduced in these mice pre-treated with SNAP-37889 prior to illumination (Fig. 6F). Interestingly, the levels of IL1-β, IL6, CCL2, and TNF-α were not changed in *Galr3*$^{-/-}$ mice exposed to light as compared to unexposed mice (Fig. 6F). Together, these results indicate that inhibition of GALR3 prevents activation of light-triggered inflammation in the retina and protects the retinal cells from apoptosis.

Depletion of *Galr3* does not affect retinal homeostasis

The effect of the depletion of GALR3-mediated signaling on normal retinal physiology was inspected in two, four, and eight-month-old *Galr3*$^{-/-}$ mice on C57BL/6J background. We examined the retina morphology, measured levels of visual receptors Rho and M cone opsin, quantified levels of 11-*cis*-retinal, and measured retina function in these mice, and compared them to the WT C57BL/6J control mice. To evaluate retina morphology we used *in vivo* SD-OCT imaging and histological analyses (Fig. 7A–C). No major differences in the retina structure and the thickness of the ONL layer were noticed between *Galr3*$^{-/-}$ mice and age-matched littermates of WT mice. The expression of Rho and cone opsin was detected in cryosections and by immunoblotting (Fig. 7D–F and Fig. S7). The overall retina morphology in *Galr3*$^{-/-}$ mice and age-matched littermates of WT mice appeared similar. The immunoblot analysis showed similar levels of Rho and M cone opsin in two-months-old *Galr3*$^{-/-}$ mice and in the WT age-matched littermates, while the levels of these receptors were slightly higher in four and eight-months-old *Galr3*$^{-/-}$ mice than in WT mice. On the other hand, levels of 11-*cis*-retinal per eye were similar in both *Galr3*$^{-/-}$ and WT age-matched littermate mice (Fig. 7G–H). These results indicate that lack of GALR3 expression has no negative effect on the expression of Rho and cone opsin receptors. The scotopic and photopic ERG responses were also very similar between agematched littermates of *Galr3*$^{-/-}$ and WT mice (Fig. 7I). Altogether, no major changes in retinal homeostasis were triggered by the depletion of the GALR3 signaling under normal physiological conditions.

Modulation of GALR3 signaling slows down photoreceptors death in retinitis pigmentosa

One of the major hallmarks of retinitis pigmentosa (RP) is retinal inflammation triggered by persistent insult associated with the abnormal genetic background that causes the death of photoreceptors. A large number of RP cases is related to mutations in Rho, the rod visual receptor. Inhibition of inflammation is one of the therapeutic possibilities to combat RP pathology [57]. GALR3 is involved in the regulation of inflammatory processes in irreversible degeneration [11, 56]. Thus, we sought to investigate if inhibition of GALR3 signaling in P23H Rho *knock-in* mice, a model of RP could slow down photoreceptor cell death. To generate P23H Rho mice genetically depleted from GALR3 ($Rho^{P23H/+}Galr3^{-/-}$ mice), we crossbred Rho P23H *knock-in* mice with $Galr3^{-/-}$ mice. Of note, both $Galr3^{-/-}$ and P23H Rho *knock-in* mice have the same C57BL/6 mouse background. Alternatively, the GALR3-mediated signaling in Rho P23H mice was inhibited with SNAP-37889, which was administered to these mice every other day from P21 to P33, according to the treatment strategy developed by us previously [58, 59]. The effect of GALR3 ablation and pharmacological inhibition on the retina structure and function was examined in 1-month-old mice at P33. The *in vivo* SD-OCT imaging and histological examination revealed substantial improvement in the thickness of the ONL layer in the retina in both $Rho^{P23H/+}Galr3^{-/-}$ mice and $Rho^{P23H/+}$ mice treated with SNAP-37889 as compared to non-treated $Rho^{P23H/+}$ mice, indicating enhanced survival of photoreceptors upon inhibition of the GALR3-mediated signaling (Fig. 8A–D). The increased levels of the visual receptors in $Rho^{P23H/+}$ mice upon pharmacological inhibition or genetic depletion of GALR3 signaling were confirmed by detecting elevated concentrations of 11-*cis*-retinal, the natural chromophore of both Rho, and cone opsins (Fig. 8E). The morphology of rod and cone photoreceptors in $Rho^{P23H/+}Galr3^{-/-}$ mice were also improved as compared to $Rho^{P23H/+}$ mice (Fig. 8F). In addition, the scotopic ERG responses were noticeably greater in $Rho^{P23H/+}Galr3^{-/-}$ and in $Rho^{P23H/+}$ mice treated with SNAP-37889 as compared to $Rho^{P23H/+}$ mice (Fig. 8H). However, blocking of GALR3 signaling only slightly changed the amplitude of the photopic ERG responses for the highest illumination intensity. Although the observed changes did not reach the levels observed in WT mice (Fig. S8), significant improvements in the retina morphology and function were noticed in $Rho^{P23H/+}$ with either genetically or pharmacologically blocked GALR3 signaling. Together our results indicate that targeting GALR3-mediated signaling should be explored as a possibility for the development of new treatment strategies against both acute and chronic retinal degeneration.

DISCUSSION

Eye degenerative diseases are associated with a disruption in retinal homeostasis, where an imbalance in the supply of nutrients and the accumulation of toxic metabolites act as pathological drivers [21]. The RPE and host immune cells, including microglia and Müller cells, are key to maintaining retina homeostasis [21, 57, 60]. These cells express various GPCRs, critical for their function, which under stress conditions could potentiate the inflammatory response aggravating the degeneration of retinal tissue [19, 22–25]. Thus, the modulation of GPCR signaling provides a well-recognized platform with neuroprotective potential. As shown before, the beneficial effects of preventing or slowing down degenerative processes in the retina could be achieved by targeting the

visual receptor rod opsin or by modulating the GPCRs associated with the activation of the cellular stress response pathways [43, 61]. In this study, we focused on the role of GALR3, a class A GPCR broadly expressed in the CNS, where its role has been associated with the modulation of inflammatory and immune responses [1]. Interestingly, GALR3 was found in the human retina, especially in the RPE cells and choroidal blood vessels, indicating that this receptor could play a role in eye homeostasis associated with signal transduction, vessel dynamics, and regulation of inflammatory processes [2, 4, 19, 26, 62]. Thus, to gain a deeper understanding of the role of GALR3 in retina degeneration, first, we investigated if GALR3 signaling is involved in the RPE cellular stress response related to the toxicity of all-*trans*-retinal, a photoproduct implicated in light-induced retina degeneration [34, 53]. We used the RPE-derived ARPE19 cell, a standard model to evaluate the toxic effect of all-*trans*-retinal and its byproducts *in vitro* [63–65]. We confirmed that GALR3 is expressed in these cells, and responds to the stimulation with GALRs-targeting small molecule ligand, galnon through the canonical signaling pathway decreasing the cellular pool of cAMP. Furthermore, we corroborated that pre-treatment of these cells with GALR3-specific antagonist SNAP-37889 blocks this signaling, similarly to other CNS-related cell models [66]. Also, we found that the effect of all-*trans*-retinal toxicity on ARPE19 cells could be modulated with a GALR3 agonist or antagonist, suggesting that GALR3-mediated signaling could be involved in the pathology of retinal degeneration. These positive *in vitro* results encouraged further *in vivo* studies to evaluate the role of GALR3 in response to stress in the retina and to examine the potential of GALR3-mediated signaling inhibition as a strategy for protecting retinal health.

First, we used $Abca4^{-/-}Rdh8^{-/-}$ mice, which lack two key enzymes involved in all-*trans*-retinal metabolism [34]. The aberrant clearance of all-*trans*-retinal results in an excessive concentration of all-*trans*-retinal and its byproducts that accumulate in the RPE and activate inflammatory responses damaging photoreceptor cells [67]. As we found in this study, the exposure of $Abca4^{-/-}Rdh8^{-/-}$ mice to intense light resulted in an increased expression of GALR3 and its ligand spexin. Remarkably, treatment of these mice with GALR3 antagonist SNAP-37889 before illumination mitigated photoreceptors damage. An inhibition of GALR3 signaling was also beneficial in WT Balb/cJ mice, which due to lack of pigmentation in the retina are susceptible to light-induced retina degeneration [68, 69]. Treatment with SNAP-37889 prior to light exposure protected retina health in these mice. Furthermore, the genetic ablation of GALR3 in WT Balb/cJ mice also decreased the susceptibility to bright light-induced retina injury.

The pathological response to excessive illumination in $Abca4^{-/-}Rdh8^{-/-}$ and WT Balb/cJ mice retinas is associated with metabolic changes and oxidative stress, followed by an enhanced expression of proinflammatory chemokines released by immune cells and activation of the apoptotic pathways [63, 70]. Interestingly, pharmacological inhibition of GALR3-mediated signaling or genetic depletion of GALR3 resulted in a decrease of the main markers associated with inflammatory stress response and prolonged the survival of photoreceptor cells. These results are in concordance with previous reports showing that modulation of inflammatory and oxidative stress response in $Abca4^{-/-}Rdh8^{-/-}$ and WT Balb/cJ mice prevent retina degeneration [44]. Importantly, under normal physiological conditions, the absence of GALR3 had no negative effects on the overall retina homeostasis,

including retina structure, the expression of the main visual receptors, and retina function. Of note, as reported by others, lack of GALR3 expression was associated with reduced levels of multiple inflammatory cytokines in immune cells residing in the skin, indicating anti-inflammatory consequences of downregulation of GALR3 signaling [11]. Also, pharmacological inhibition of GALR3 ameliorated inflammation in acute pancreatitis [12]. Thus, the results obtained in the light-induced retina damage models encouraged us to evaluate GALR3 as a possible therapeutic target in RP-linked retina degeneration, in which inflammatory responses are triggered by the continuous insult of inherited mutation. The underlying mechanism of RP pathology and the progression of photoreceptor death remains not fully understood. However, the accumulation of misfolded Rho in the ER membranes, which triggers activation of the unfolded protein response (UPR) is the major hallmark of Rho-associated RP [40, 71, 72]. In addition, degenerating rods cause a decrease in oxygen consumption, resulting in an excess of oxygen in the outer retina that leads to an increase in the concentration of redox species in this tissue [40]. The imbalance of redox species and activation of stress signaling pathways activating apoptosis are common features of light-induced and RP retina pathologies. Of note, in hypothalamic neurons, increased concentration of redox species triggered the ER stress response inducing the activation of Bax/Bcl2-related cell death, which correlated with an enhanced expression of GALR2, GALR3, and spexin in these neurons [73]. Remarkably, in the RP-related mouse model carrying the P23H mutation in Rho, both the treatment with GALR3 antagonist and genetic ablation of this receptor enhanced the survival of photoreceptors. Retina function and morphology of rod and cone photoreceptors in $Rho^{P23H/+}Galr3^{-/-}$ and $Rho^{P23H/+}$ mice treated with GALR3 inhibitor were greatly improved as compared to $Rho^{P23H/+}$ mice. Of note, the slightly lesser effect of the pharmacological inhibition as compared to the genetic ablation of GALR3 may suggest that the dosing regimen could be optimized or novel GALR3 inhibitors could be evaluated for a better outcome. Together, for the first time, we have demonstrated that GALR3-mediated signaling could be implicated in the progression of degenerative pathologies in the retina. The beneficial effects related to the negative modulation of GALR3 signaling could be associated with a decrease in the overall activation of stress response cellular pathways and reduced levels of inflammatory responses. Thus, the results presented in this work point out GALR3 as a possible target to explore for the development of new treatment strategies for both acute and chronic retinopathies.

The GALRs signaling is complex. It not only involves three receptors GALR1–3, but these receptors can form homo and hetero-dimers, which increases the challenge to study the molecular signaling of GALRs in detail in a specific tissue [74–76]. Moreover, despite GALR3, also GALR2 is expressed in the retina, which may hinder full data interpretation. Therefore, there is a need for a follow-up study examining the effect of GALR2 inhibition on retina pathologies. Also, the development of novel GALR3 analogs with high specificity would validate the results presented here.

In conclusion, based on the results presented in this work, for the first time we showed that GALR3 could play a pivotal role in the pathological onset of acute and chronic retinopathies. Therefore, the potential of GALR3 as a target for the development of treatments against retina degenerative diseases should be further investigated.

Supplementary Material

Refer to Web version on PubMed Central for supplementary material.

ACKNOWLEDGEMENTS

This research was supported partially by grants from the National Institute of Health (NIH) (EY032874 to B.J.). The authors thank the Visual Science Research Center Core at Case Western Reserve University (supported by the NIH grant P30 EY011373) with special gratitude directed to Catherine Doller for assistance with mouse eye tissue sectioning and H&E staining, Dawn Doller for preparing mouse eye cryosections, and Maryanne Pendergast for assistance in slide imaging. We thank Dr. Marcin Golczak for measuring the light spectrum of the bulbs used in the light damage experiments.

ABBREVIATIONS

adRP	autosomal dominant retinitis pigmentosa
AF	autofluorescence
AMD	age-related macular degeneration
bw(s)	body weight(s)
cAMP	cyclic adenosine monophosphate
ER	endoplasmic reticulum
ERG	electroretinography
DAPI	4’6’-diamidino-2-phenyl-indole
DMSO	dimethyl sulfoxide
GPCR	G protein-coupled receptor
INL	inner nuclear layer
ONH	optic nerve head
ONL	outer nuclear layer
PNA	peanut agglutinin
ROS	rod outer segments
RP	retinitis pigmentosa
RPE	retinal pigment epithelium
RT	room temperature
S.D.	standard deviation
SD-OCT	spectral domain-optic coherence tomography
SLO	scanning laser ophthalmoscopy

WT wild type

REFERENCES

1. Gopalakrishnan L, Chatterjee O, Raj C, Pullimamidi D, Advani J, Mahadevan A, Keshava Prasad TS: An assembly of galanin-galanin receptor signaling network. J Cell Commun Signal 2021, 15(2):269–275. [PubMed: 33136286]
2. Webling KE, Runesson J, Bartfai T, Langel U: Galanin receptors and ligands. Front Endocrinol (Lausanne) 2012, 3:146. [PubMed: 23233848]
3. Robinson JK, Bartfai T, Langel U: Galanin/GALP receptors and CNS homeostatic processes. CNS Neurol Disord Drug Targets 2006, 5(3):327–334. [PubMed: 16787232]
4. Kim DK, Yun S, Son GH, Hwang JI, Park CR, Kim JI, Kim K, Vaudry H, Seong JY: Coevolution of the spexin/galanin/kisspeptin family: Spexin activates galanin receptor type II and III. Endocrinology 2014, 155(5):1864–1873. [PubMed: 24517231]
5. Abramov U, Floren A, Echevarria DJ, Brewer A, Manuzon H, Robinson JK, Bartfai T, Vasar E, Langel U: Regulation of feeding by galnon. Neuropeptides 2004, 38(1):55–61. [PubMed: 15003717]
6. Lang R, Gundlach AL, Kofler B: The galanin peptide family: receptor pharmacology, pleiotropic biological actions, and implications in health and disease. Pharmacol Ther 2007, 115(2):177–207. [PubMed: 17604107]
7. Kiezun J, Godlewski J, Krazinski BE, Kozielec Z, Kmiec Z: Galanin Receptors (GalR1, GalR2, and GalR3) Expression in Colorectal Cancer Tissue and Correlations to the Overall Survival and Poor Prognosis of CRC Patients. Int J Mol Sci 2022, 23(7).
8. Belfer I, Hipp H, Bollettino A, McKnight C, Evans C, Virkkunen M, Albaugh B, Max MB, Goldman D, Enoch MA: Alcoholism is associated with GALR3 but not two other galanin receptor genes. Genes Brain Behav 2007, 6(5):473–481. [PubMed: 17083333]
9. Mansouri S, Barde S, Ortsater H, Eweida M, Darsalia V, Langel U, Sjoholm A, Hokfelt T, Patrone C: GalR3 activation promotes adult neural stem cell survival in response to a diabetic milieu. J Neurochem 2013, 127(2):209–220. [PubMed: 23927369]
10. Freimann K, Kurrikoff K, Langel U: Galanin receptors as a potential target for neurological disease. Expert Opin Ther Targets 2015, 19(12):1665–1676. [PubMed: 26220265]
11. Locker F, Vidali S, Holub BS, Stockinger J, Brunner SM, Ebner S, Koller A, Trost A, Reitsamer HA, Schwarzenbacher D et al. : Lack of Galanin Receptor 3 Alleviates Psoriasis by Altering Vascularization, Immune Cell Infiltration, and Cytokine Expression. J Invest Dermatol 2018, 138(1):199–207. [PubMed: 28844939]
12. Barreto SG, Bazargan M, Zotti M, Hussey DJ, Sukocheva OA, Peiris H, Leong M, Keating DJ, Schloithe AC, Carati CJ et al. : Galanin receptor 3--a potential target for acute pancreatitis therapy. Neurogastroenterol Motil 2011, 23(3):e141–151. [PubMed: 21303427]
13. Fang P, Yu M, Wan D, Zhang L, Han L, Shen Z, Shi M, Zhu Y, Zhang Z, Bo P: Regulatory effects of galanin system on development of several age-related chronic diseases. Exp Gerontol 2017, 95:88–97. [PubMed: 28450241]
14. Botz B, Kemeny A, Brunner SM, Sternberg F, Csepregi J, Mocsai A, Pinter E, McDougall JJ, Kofler B, Helyes Z: Lack of Galanin 3 Receptor Aggravates Murine Autoimmune Arthritis. J Mol Neurosci 2016, 59(2):260–269. [PubMed: 26941032]
15. Crawley JN: Galanin impairs cognitive abilities in rodents: relevance to Alzheimer's disease. Exp Suppl 2010, 102:133–141. [PubMed: 21299066]
16. Swanson CJ, Blackburn TP, Zhang X, Zheng K, Xu ZQ, Hokfelt T, Wolinsky TD, Konkel MJ, Chen H, Zhong H et al. : Anxiolytic- and antidepressant-like profiles of the galanin-3 receptor (Gal3) antagonists SNAP 37889 and SNAP 398299. Proc Natl Acad Sci U S A 2005, 102(48):17489-17494.
17. Ash BL, Quach T, Williams SJ, Lawrence AJ, Djouma E: Galanin-3 receptor antagonism by SNAP 37889 reduces motivation to self-administer alcohol and attenuates cue-induced reinstatement of alcohol-seeking in iP rats. J Pharmacol Sci 2014, 125(2):211–216. [PubMed: 24881957]

18. Scheller KJ, Williams SJ, Lawrence AJ, Djouma E: The galanin-3 receptor antagonist, SNAP 37889, suppresses alcohol drinking and morphine self-administration in mice. Neuropharmacology 2017, 118:1–12. [PubMed: 28274821]
19. Schrodl F, Kaser-Eichberger A, Trost A, Strohmaier C, Bogner B, Runge C, Bruckner D, Motloch K, Holub B, Kofler B et al. : Distribution of galanin receptors in the human eye. Exp Eye Res 2015, 138:42–51. [PubMed: 26122049]
20. Troger J, Kieselbach G, Teuchner B, Kralinger M, Nguyen QA, Haas G, Yayan J, Gottinger W, Schmid E: Peptidergic nerves in the eye, their source and potential pathophysiological relevance. Brain Res Rev 2007, 53(1):39–62. [PubMed: 16872680]
21. Wong-Riley MT: Energy metabolism of the visual system. Eye Brain 2010, 2:99–116. [PubMed: 23226947]
22. Figueroa AG, McKay BS: A G-Protein Coupled Receptor and Macular Degeneration. Cells 2020, 9(4).
23. Chang Q, Chen S, Yang T: The GPCR Antagonistic Drug CM-20 Stimulates Mitochondrial Activity in Human RPE Cells. Open Biochem J 2022, 16.
24. Saddala MS, Lennikov A, Mukwaya A, Yang X, Tang S, Huang H: Data mining and network analysis reveals C-X-C chemokine receptor type 5 is involved in the pathophysiology of age-related macular degeneration. J Biomol Struct Dyn 2021:1–10.
25. Figueroa AG, McKay BS: GPR143 Signaling and Retinal Degeneration. Adv Exp Med Biol 2019, 1185:15–19. [PubMed: 31884582]
26. Kaser-Eichberger A, Trost A, Strohmaier C, Bogner B, Runge C, Bruckner D, Hohberger B, Junemann A, Kofler B, Reitsamer HA et al. : Distribution of the neuro-regulatory peptide galanin in the human eye. Neuropeptides 2017, 64:85–93. [PubMed: 27914762]
27. Porzionato A, Rucinski M, Macchi V, Stecco C, Malendowicz LK, De Caro R: Spexin expression in normal rat tissues. J Histochem Cytochem 2010, 58(9):825–837. [PubMed: 20530460]
28. Kofler B, Brunner S, Koller A, Wiesmayr S, Locker F, Lang R, Botz B, Kemeny A, Helyes Z: Contribution of the galanin system to inflammation. Springerplus 2015, 4(Suppl 1):L57. [PubMed: 27386220]
29. Locker F, Lang AA, Koller A, Lang R, Bianchini R, Kofler B: Galanin modulates human and murine neutrophil activation in vitro. Acta Physiol (Oxf) 2015, 213(3):595–602. [PubMed: 25545502]
30. Kaur G, Singh NK: Inflammation and retinal degenerative diseases. Neural Regen Res 2023, 18(3):513–518. [PubMed: 36018156]
31. Chen Y, Palczewska G, Masuho I, Gao S, Jin H, Dong Z, Gieser L, Brooks MJ, Kiser PD, Kern TS et al. : Synergistically acting agonists and antagonists of G protein-coupled receptors prevent photoreceptor cell degeneration. Sci Signal 2016, 9(438):ra74. [PubMed: 27460988]
32. Leinonen H, Choi EH, Gardella A, Kefalov VJ, Palczewski K: A Mixture of U.S. Food and Drug Administration-Approved Monoaminergic Drugs Protects the Retina From Light Damage in Diverse Models of Night Blindness. Invest Ophthalmol Vis Sci 2019, 60(5):1442–1453. [PubMed: 30947334]
33. Maeda A, Golczak M, Maeda T, Palczewski K: Limited roles of Rdh8, Rdh12, and Abca4 in all-trans-retinal clearance in mouse retina. Invest Ophthalmol Vis Sci 2009, 50(11):5435–5443. [PubMed: 19553623]
34. Chen Y, Okano K, Maeda T, Chauhan V, Golczak M, Maeda A, Palczewski K: Mechanism of all-trans-retinal toxicity with implications for stargardt disease and age-related macular degeneration. J Biol Chem 2012, 287(7):5059–5069. [PubMed: 22184108]
35. Rashid K, Akhtar-Schaefer I, Langmann T: Microglia in Retinal Degeneration. Front Immunol 2019, 10:1975.
36. Ambati J, Fowler BJ: Mechanisms of age-related macular degeneration. Neuron 2012, 75(1):26–39. [PubMed: 22794258]
37. Fritsche LG, Fariss RN, Stambolian D, Abecasis GR, Curcio CA, Swaroop A: Age-related macular degeneration: genetics and biology coming together. Annu Rev Genomics Hum Genet 2014, 15:151–171. [PubMed: 24773320]

38. Hartong DT, Berson EL, Dryja TP: Retinitis pigmentosa. Lancet 2006, 368(9549):1795–1809. [PubMed: 17113430]
39. Nguyen AT, Campbell M, Kiang AS, Humphries MM, Humphries P: Current therapeutic strategies for P23H RHO-linked RP. Adv Exp Med Biol 2014, 801:471–476. [PubMed: 24664733]
40. Athanasiou D, Aguila M, Bellingham J, Li W, McCulley C, Reeves PJ, Cheetham ME: The molecular and cellular basis of rhodopsin retinitis pigmentosa reveals potential strategies for therapy. Prog Retin Eye Res 2018, 62:1–23. [PubMed: 29042326]
41. Scheller KJ, Williams SJ, Lawrence AJ, Jarrott B, Djouma E: An improved method to prepare an injectable microemulsion of the galanin-receptor 3 selective antagonist, SNAP 37889, using Kolliphor((R)) HS 15. MethodsX 2014, 1:212–216. [PubMed: 26150955]
42. Kim SR, Fishkin N, Kong J, Nakanishi K, Allikmets R, Sparrow JR: Rpe65 Leu450Met variant is associated with reduced levels of the retinal pigment epithelium lipofuscin fluorophores A2E and iso-A2E. Proc Natl Acad Sci U S A 2004, 101(32):11668–11672. [PubMed: 15277666]
43. Gao S, Parmar T, Palczewska G, Dong Z, Golczak M, Palczewski K, Jastrzebska B: Protective Effect of a Locked Retinal Chromophore Analog against Light-Induced Retinal Degeneration. Mol Pharmacol 2018, 94(4):1132–1144. [PubMed: 30018116]
44. Ortega JT, Parmar T, Golczak M, Jastrzebska B: Protective Effects of Flavonoids in Acute Models of Light-Induced Retinal Degeneration. Mol Pharmacol 2021, 99(1):60–77. [PubMed: 33154094]
45. Sakami S, Maeda T, Bereta G, Okano K, Golczak M, Sumaroka A, Roman AJ, Cideciyan AV, Jacobson SG, Palczewski K: Probing mechanisms of photoreceptor degeneration in a new mouse model of the common form of autosomal dominant retinitis pigmentosa due to P23H opsin mutations. J Biol Chem 2011, 286(12):10551–10567. [PubMed: 21224384]
46. Ortega JT, Parmar T, Carmena-Bargueno M, Perez-Sanchez H, Jastrzebska B: Flavonoids improve the stability and function of P23H rhodopsin slowing down the progression of retinitis pigmentosa in mice. J Neurosci Res 2022.
47. Palczewski K, Van Hooser JP, Garwin GG, Chen J, Liou GI, Saari JC: Kinetics of visual pigment regeneration in excised mouse eyes and in mice with a targeted disruption of the gene encoding interphotoreceptor retinoid-binding protein or arrestin. Biochemistry 1999, 38(37):12012–12019. [PubMed: 10508404]
48. Garwin GG, Saari JC: High-performance liquid chromatography analysis of visual cycle retinoids. Methods Enzymol 2000, 316:313–324. [PubMed: 10800683]
49. Boussif O, Lezoualc'h F, Zanta MA, Mergny MD, Scherman D, Demeneix B, Behr JP: A versatile vector for gene and oligonucleotide transfer into cells in culture and in vivo: polyethylenimine. Proc Natl Acad Sci USA 1995, 92(16):7297–7301. [PubMed: 7638184]
50. Chen Y, Tang H: High-throughput screening assays to identify small molecules preventing photoreceptor degeneration caused by the rhodopsin P23H mutation. Methods Mol Biol 2015, 1271:369–390. [PubMed: 25697536]
51. Mosmann T: Rapid colorimetric assay for cellular growth and survival: application to proliferation and cytotoxicity assays. J Immunol Methods 1983, 65(1–2):55–63. [PubMed: 6606682]
52. Wu Y, Fishkin NE, Pande A, Pande J, Sparrow JR: Novel lipofuscin bisretinoids prominent in human retina and in a model of recessive Stargardt disease. J Biol Chem 2009, 284(30):20155–20166.
53. Maeda T, Golczak M, Maeda A: Retinal photodamage mediated by all-trans-retinal. Photochem Photobiol 2012, 88(6):1309–1319. [PubMed: 22428905]
54. Holz FG, Schutt F, Kopitz J, Eldred GE, Kruse FE, Volcker HE, Cantz M: Inhibition of lysosomal degradative functions in RPE cells by a retinoid component of lipofuscin. Invest Ophthalmol Vis Sci 1999, 40(3):737–743. [PubMed: 10067978]
55. Sparrow JR, Nakanishi K, Parish CA: The lipofuscin fluorophore A2E mediates blue light-induced damage to retinal pigmented epithelial cells. Invest Ophthalmol Vis Sci 2000, 41(7):1981–1989. [PubMed: 10845625]
56. Botz B, Kemeny A, Brunner SM, Locker F, Csepregi J, Mocsai A, Pinter E, McDougall JJ, Kofler B, Helyes Z: Lack of Galanin 3 Receptor Aggravates Murine Autoimmune Arthritis. J Mol Neurosci 2016, 59(2):260–269. [PubMed: 26941032]

57. Ortega JT, Jastrzebska B: Neuroinflammation as a Therapeutic Target in Retinitis Pigmentosa and Quercetin as Its Potential Modulator. Pharmaceutics 2021, 13(11).
58. Ortega JT, Parmar T, Carmena-Bargueno M, Perez-Sanchez H, Jastrzebska B: Flavonoids improve the stability and function of P23H rhodopsin slowing down the progression of retinitis pigmentosa in mice. J Neurosci Res 2022, 100(4):1063–1083. [PubMed: 35165923]
59. Ortega JT, McKee AG, Roushar FJ, Penn WD, Schlebach JP, Jastrzebska B: Chromenone derivatives as novel pharmacological chaperones for retinitis pigmentosa-linked rod opsin mutants. Hum Mol Genet 2022.
60. Davies LC, Jenkins SJ, Allen JE, Taylor PR: Tissue-resident macrophages. Nat Immunol 2013, 14(10):986–995. [PubMed: 24048120]
61. Chen Y, Palczewska G, Mustafi D, Golczak M, Dong Z, Sawada O, Maeda T, Maeda A, Palczewski K: Systems pharmacology identifies drug targets for Stargardt disease-associated retinal degeneration. J Clin Invest 2013, 123(12):5119–5134. [PubMed: 24231350]
62. Celik F, Aydin S: Blood and aqueous humor phoenixin, endocan and spexin in patients with diabetes mellitus and cataract with and without diabetic retinopathy. Peptides 2022, 150:170728.
63. Sawada O, Perusek L, Kohno H, Howell SJ, Maeda A, Matsuyama S, Maeda T: All-trans-retinal induces Bax activation via DNA damage to mediate retinal cell apoptosis. Exp Eye Res 2014, 123:27–36. [PubMed: 24726920]
64. Poliakov E, Strunnikova NV, Jiang JK, Martinez B, Parikh T, Lakkaraju A, Thomas C, Brooks BP, Redmond TM: Multiple A2E treatments lead to melanization of rod outer segment-challenged ARPE-19 cells. Mol Vis 2014, 20:285–300. [PubMed: 24644403]
65. Shi Q, Wang Q, Li J, Zhou X, Fan H, Wang F, Liu H, Sun X, Sun X: A2E Suppresses Regulatory Function of RPE Cells in Th1 Cell Differentiation Via Production of IL-1beta and Inhibition of PGE2. Invest Ophthalmol Vis Sci 2015, 56(13):7728–7738. [PubMed: 26641550]
66. Koller A, Rid R, Beyreis M, Bianchini R, Holub BS, Lang A, Locker F, Brodowicz B, Velickovic O, Jakab M et al. : In vitro toxicity of the galanin receptor 3 antagonist SNAP 37889. Neuropeptides 2016, 56:83–88. [PubMed: 26725588]
67. Maeda A, Maeda T, Golczak M, Palczewski K: Retinopathy in mice induced by disrupted all-trans-retinal clearance. J Biol Chem 2008, 283(39):26684–26693. [PubMed: 18658157]
68. LaVail MM, Gorrin GM, Repaci MA, Yasumura D: Light-induced retinal degeneration in albino mice and rats: strain and species differences. Prog Clin Biol Res 1987, 247:439–454. [PubMed: 3685038]
69. LaVail MM, Gorrin GM, Repaci MA: Strain differences in sensitivity to light-induced photoreceptor degeneration in albino mice. Curr Eye Res 1987, 6(6):825–834. [PubMed: 3608569]
70. Parmar T, Parmar VM, Perusek L, Georges A, Takahashi M, Crabb JW, Maeda A: Lipocalin 2 Plays an Important Role in Regulating Inflammation in Retinal Degeneration. J Immunol 2018, 200(9):3128–3141. [PubMed: 29602770]
71. Chiang WC, Kroeger H, Sakami S, Messah C, Yasumura D, Matthes MT, Coppinger JA, Palczewski K, LaVail MM, Lin JH: Robust Endoplasmic Reticulum-Associated Degradation of Rhodopsin Precedes Retinal Degeneration. Mol Neurobiol 2015, 52(1):679–695. [PubMed: 25270370]
72. Gorbatyuk MS, Starr CR, Gorbatyuk OS: Endoplasmic reticulum stress: New insights into the pathogenesis and treatment of retinal degenerative diseases. Prog Retin Eye Res 2020, 79:100860.
73. Tran A, Loganathan N, McIlwraith EK, Belsham DD: Palmitate and Nitric Oxide Regulate the Expression of Spexin and Galanin Receptors 2 and 3 in Hypothalamic Neurons. Neuroscience 2020, 447:41–52. [PubMed: 31730796]
74. Wirz SA, Davis CN, Lu X, Zal T, Bartfai T: Homodimerization and internalization of galanin type 1 receptor in living CHO cells. Neuropeptides 2005, 39(6):535–546. [PubMed: 16242774]
75. De Oliveira PA, Moreno E, Casajuana-Martin N, Casado-Anguera V, Cai NS, Camacho-Hernandez GA, Zhu H, Bonifazi A, Hall MD, Weinshenker D et al. : Preferential Gs protein coupling of the galanin Gal1 receptor in the micro-opioid-Gal1 receptor heterotetramer. Pharmacol Res 2022, 182:106322.

76. Tena-Campos M, Ramon E, Lupala CS, Perez JJ, Koch KW, Garriga P: Zinc Is Involved in Depression by Modulating G Protein-Coupled Receptor Heterodimerization. Mol Neurobiol 2016, 53(3):2003–2015. [PubMed: 25855059]

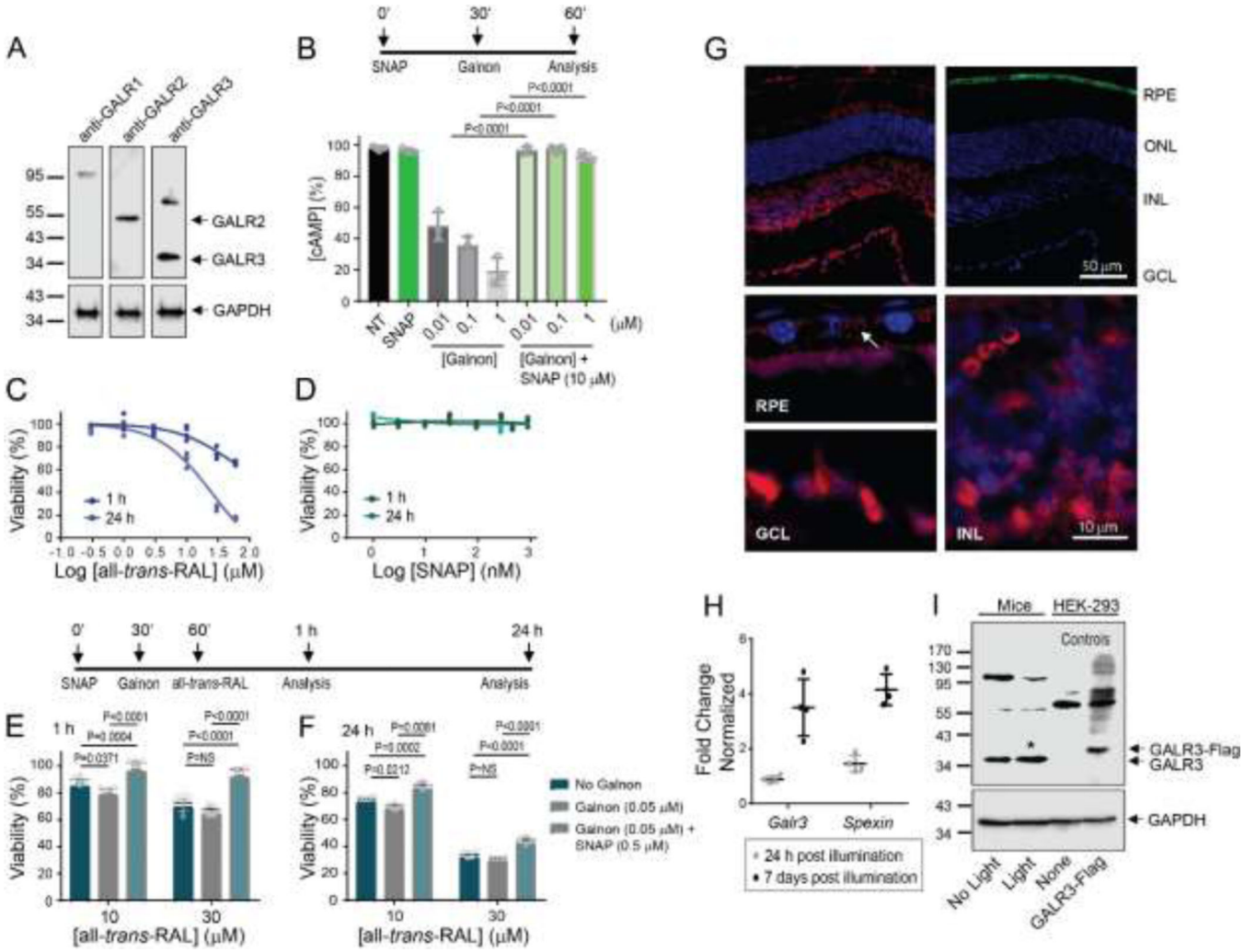

Figure 1. Modulation of GALR3 signaling in the RPE-derived cells and the GALR3 expression in the mouse retina.

A, The expression of GALR2 and GALR3, but not GALR1 was detected in the protein extract prepared from the ARPE19 cells. The upper bands ~100 KDa detected with an anti-GALR1 antibody and ~70 KDa detected with an anti-GALR3 antibody are most likely unspecific. The representative immunoblots are shown. **B**, An inhibition of GALR3 with its specific antagonist SNAP-3788 modulates negatively signaling in the ARPE19 cells stimulated with galnon agonist. **C-D**, Cytotoxicity of all-*trans*-retinal and SNAP-3788 examined in the ARPE19 cells, respectively. Cells were treated with various doses of each compound for 1 h or 24 h and their effect on cell viability was determined. **E-F**, The effect of treatment with SNAP-3788 (0.5 μM) on the viability of the ARPE19 cells exposed to all-*trans*-retinal (at 10 and 30 μM) for 1 h or 24 h, which were stimulated with galnon (0.05 μM) prior to all-*trans*-retinal stress. Error bars represent standard deviation (S.D.). Statistically different changes are shown in the figure. **G**, GALR3-immunoreactivity (red) was detected on cryosections of *Abca4*$^{-/-}$*Rdh8*$^{-/-}$ mouse eyes, in the inner nuclear layer (INL), ganglion cells, and in the retinal pigment epithelium (RPE). RPE cells were also labeled with monoclonal anti-RPE65 protein (green) antibody. **H**, The RT-qPCR analysis of

the expression of *Galr3* and its native agonist *Spexin* in the eyes of *Abca4*$^{-/-}$*Rdh8*$^{-/-}$ mice exposed to bright light detected 24 h and 7 days after illumination. The expression of these genes was normalized to the expression of *Gapdh*. The mean of data from three independent experiments is shown as a fold change of these genes expression in dark-adapted mice. **I**, Immunoblot analyses assessing the changes in the GALR3 expression in the eyes of *Abca4*$^{-/-}$*Rdh8*$^{-/-}$ mice exposed to bright light insult 7 days after illumination. The protein extracts from the HEK-293 cells and HEK-293 cells transfected with the GALR3-Flag expressing vector were used as controls. The representative immunoblot is shown. Statistical analyses were performed with the two-way ANOVA and post hoc Turkey's tests.

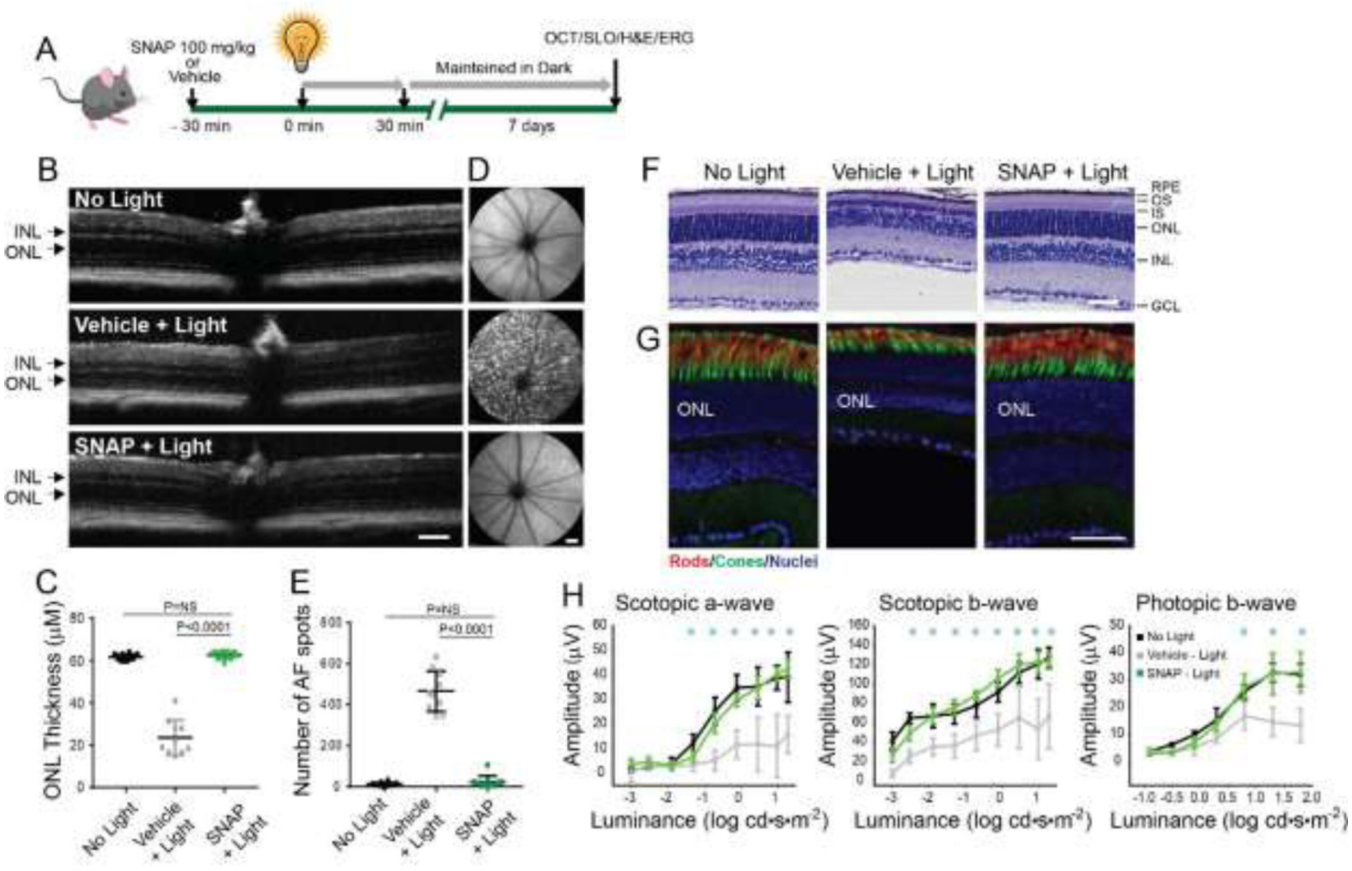

Figure 2. Inhibition of GALR3 protects the retina from light-induced degeneration in *Abca4*$^{-/-}$*Rdh8*$^{-/-}$ mice.

A, Experimental design. *Abca4*$^{-/-}$*Rdh8*$^{-/-}$ mice were used to examine the effect of pharmacological inhibition of GALR3. These mice were treated with a single dose of GALR3 specific inhibitor SNAP-37889 30 min before illumination for 30 min and then maintained in the dark for 7 days before analyses. These mice exhibit sensitivity to bright light and develop severe retina degeneration within a few days after illumination. **B**, The representative images of the retina that were visualized with the spectral domain optical coherence tomography (SD-OCT). Scale bar 100 μm. **C**, The measurement of the outer nuclear layer (ONL) thickness at 500 μm from the optic nerve head (ONH). The measurement was performed in n = 6 mice per group. Statistically different changes were observed between vehicle-treated mice and dark-adapted mice, and in SNAP-37889-treated mice compared to vehicle-treated mice. No statistical difference was found between dark-adapted and drug-treated mice. Error bars indicate standard deviation (S.D.). *P* values for the statistically different changes ($P < 0.05$) are indicated in the figure. **D**, The representative scanning laser ophthalmoscopy (SLO) images of the whole fundus. The autofluorescence (AF) spots were detected in vehicle-treated mice. Scale bar 1 mm. **E**, Quantification of the AF spots performed in n = 6 mice per group. Statistically different changes were observed in vehicle-treated mice compared to dark-adapted mice and between the drug- and vehicle-treated mice. No statistical difference was found for dark-adapted and SNAP-37889-treated mice. Error bars indicate S.D. The *P* values for the statistically different changes ($P < 0.05$)

are indicated in the figure. **F**, The retinal structure was inspected in the hematoxylin and eosin (H&E)-stained paraffin eye sections. Scale bar 50 μm. **G**, The retinal cryosections labeled with anti-Rho antibody to detect rod photoreceptors (red) and peanut agglutinin (PNA) to detect cone photoreceptors (green). Nuclei were stained with DAPI (blue). Scale bar 25 μm. **H**, Retinal function was assessed by measuring the electroretinography (ERG) responses. ERG measurements were performed in n = 5 mice per treatment group. Both a-wave and b-wave responses were protected by SNAP-37889 treatment prior to light exposure as compared to vehicle-treated mice. These changes were statistically different. No statistical difference was found for dark-adapted and SNAP-37889-treated mice. Error bars indicate S.D. Statistically different changes ($P < 0.05$) in the ERG responses upon treatment with SNAP-37889 compared to vehicle-treated mice are indicated with asterisks. Statistical analyses were performed with the two-way ANOVA and post hoc Turkey's tests. IS, inner segments; OS, outer segments; INL, inner nuclear layer; GCL, ganglion cell layer; RPE, retinal pigment epithelium; NS, not statistically significant.

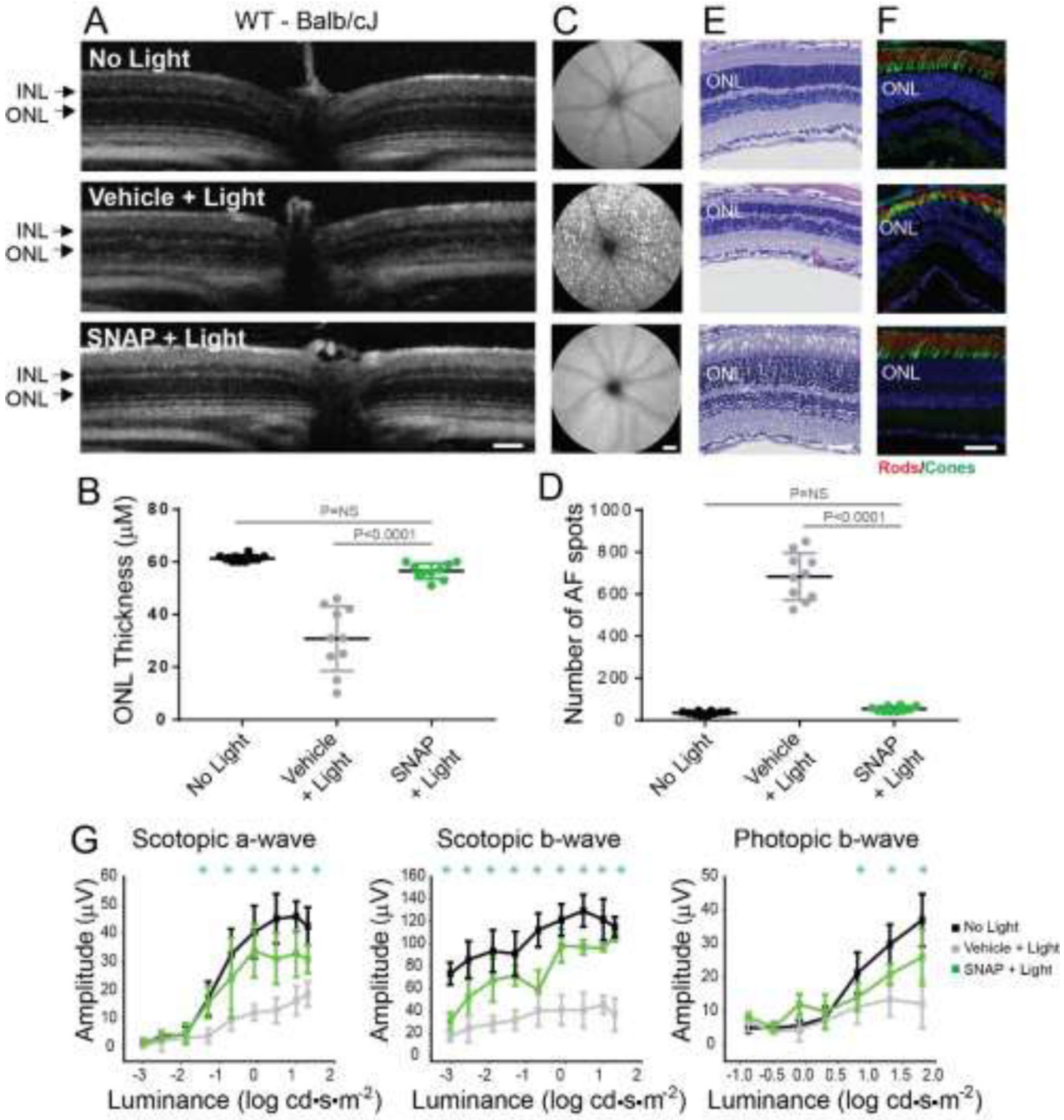

Figure 3. Inhibition of GALR3 protects the retina from light-induced degeneration in WT mice.

Balb/cJ mice, susceptible to retina damage with bright light were examined. These mice were treated with a single dose of SNAP-37889, a GALR3-specific antagonist 30 min before illumination for 60 min and then maintained in the dark for 7 days before analyses. **A**, The representative spectral domain optical coherence tomography (SD-OCT) images of the retina. Scale bar 100 μm. **B**, The measurement of the outer nuclear layer (ONL) thickness at 500 μm from the optic nerve head (ONH). The measurement was performed in n = 6 mice per group. Statistically different changes were observed between vehicle-treated and

dark-adapted mice, and in SNAP-37889-treated mice compared to vehicle-treated mice. No statistical difference was found between dark-adapted and drug-treated mice. Error bars indicate standard deviation (S.D.). *P* values for the statistically different changes ($P < 0.05$) are indicated in the figure. **C**, The representative scanning laser ophthalmoscopy (SLO) images of the whole fundus. The autofluorescence (AF) spots were detected in vehicle-treated mice. Scale bar 1 mm. **D**, Quantification of the AF spots was performed in n = 6 mice per group. Statistically different changes were observed between vehicle-treated mice compared to dark-adapted mice, and the drug- and vehicle-treated mice. No statistical difference was found for dark-adapted and SNAP-37889-treated mice. Error bars indicate S.D. The *P* values for the statistically different changes ($P < 0.05$) are indicated in the figure. **E**, The retinal structure was examined in the hematoxylin and eosin (H&E)-stained paraffin eye sections. Scale bar 50 μm. **F**, The retinal cryosections labeled with anti-Rho antibody to detect rod photoreceptors (red) and peanut agglutinin (PNA) to detect cone photoreceptors (green). Nuclei were stained with DAPI (blue). Scale bar 25 μm. **G**, Retinal function was assessed by measuring the electroretinography (ERG) responses performed in n = 5 mice per treatment group. Both a-wave and b-wave responses were protected by SNAP-37889 administered prior to illumination as compared to vehicle-treated mice. These changes were statistically different. No statistical difference was found for dark-adapted and SNAP-37889-treated mice. Error bars indicate S.D. Statistically different changes ($P < 0.05$) in the ERG responses upon treatment with SNAP-37889 compared to vehicle-treated mice are indicated with asterisks. Statistical analyses were performed with the two-way ANOVA and post hoc Turkey's tests. NS, not statistically significant.

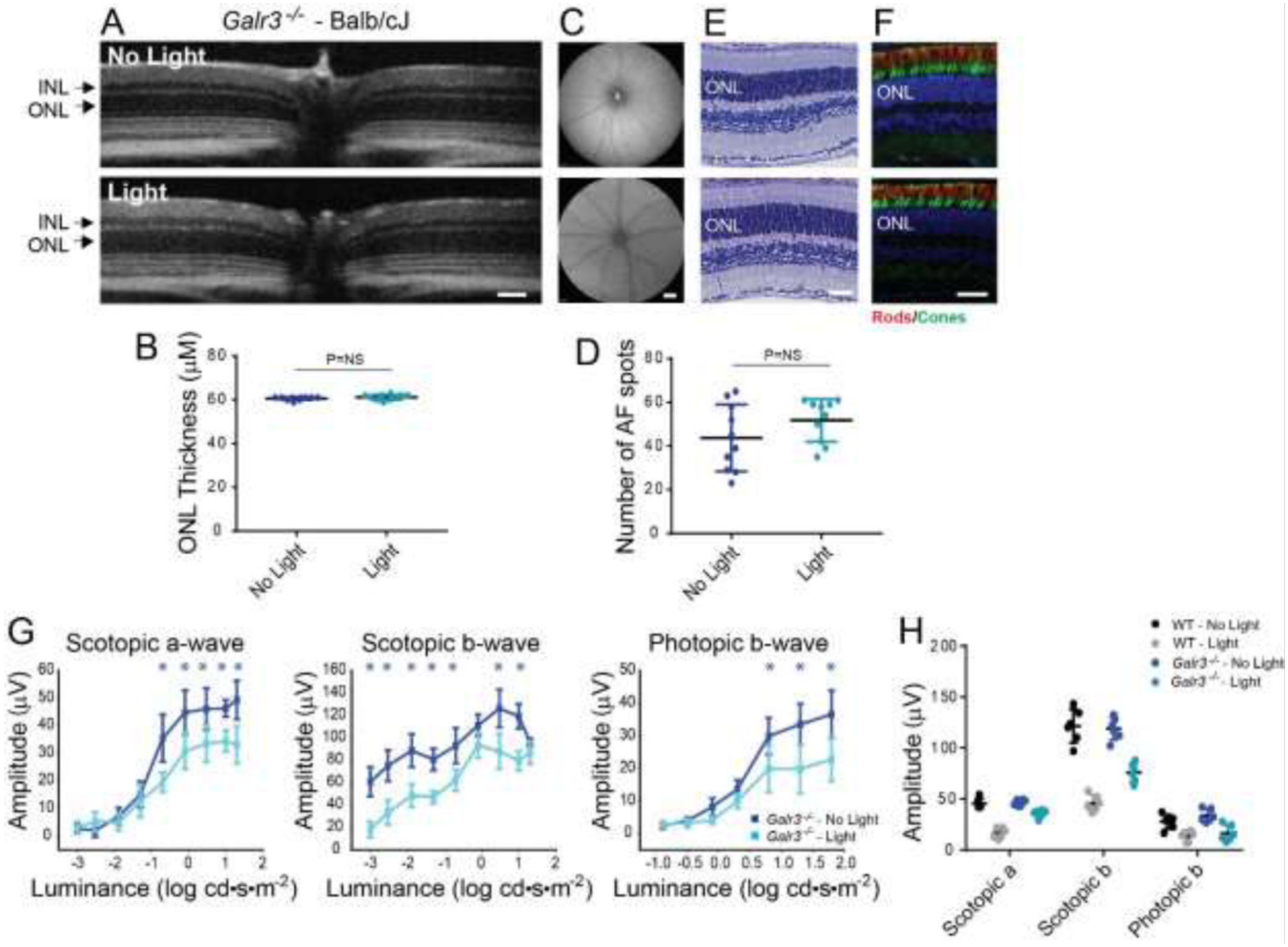

Figure 4. Lack of *Galr3* protects the retina from light-induced degeneration.

Galr3$^{-/-}$ were crossbred with Balb/cJ mice to generate *Galr3* knockout mice susceptible to bright light-induced retina injury. **A**, The representative spectral domain optical coherence tomography (SD-OCT) images of the retina of dark-adapted and illuminated mice. Scale bar 100 μm. **B**, The measurement of the outer nuclear layer (ONL) thickness at 500 μm from the optic nerve head (ONH). The measurement was performed in n = 6 mice per group. Error bars indicate standard deviation (S.D.). No statistically different changes were observed between these mice. **C**, The representative scanning laser ophthalmoscopy (SLO) images of the whole fundus. The autofluorescence (AF) spots were not detected in light-exposed mice. Scale bar 1 mm. **D**, Quantification of the AF spots performed in n = 6 mice per group. Error bars indicate S.D. No statistically different changes were observed between these mice. **E**, The retinal morphology was examined in the hematoxylin and eosin (H&E)-stained paraffin eye sections. Scale bar 50 μm. **F**, The retinal cryosections labeled with anti-Rho antibody to detect rod photoreceptors (red) and peanut agglutinin (PNA) to detect cone photoreceptors (green). Nuclei were stained with DAPI (blue). Scale bar 25 μm. **G**, Retinal function was assessed by measuring the electroretinography (ERG) responses performed in n = 5 mice per group. Error bars indicate S.D. **H**, The ERG response amplitude at 1 μV for scotopic a- and b-waves, and at 1.3 μV for photopic b-wave extracted from figures 3G and 4G to

compare the responses of WT and *Galr3*$^{-/-}$ mice. Statistically different changes ($P < 0.05$) are indicated with asterisks. Statistical analyses were performed with the two-way ANOVA and post hoc Turkey's tests. NS, not statistically significant.

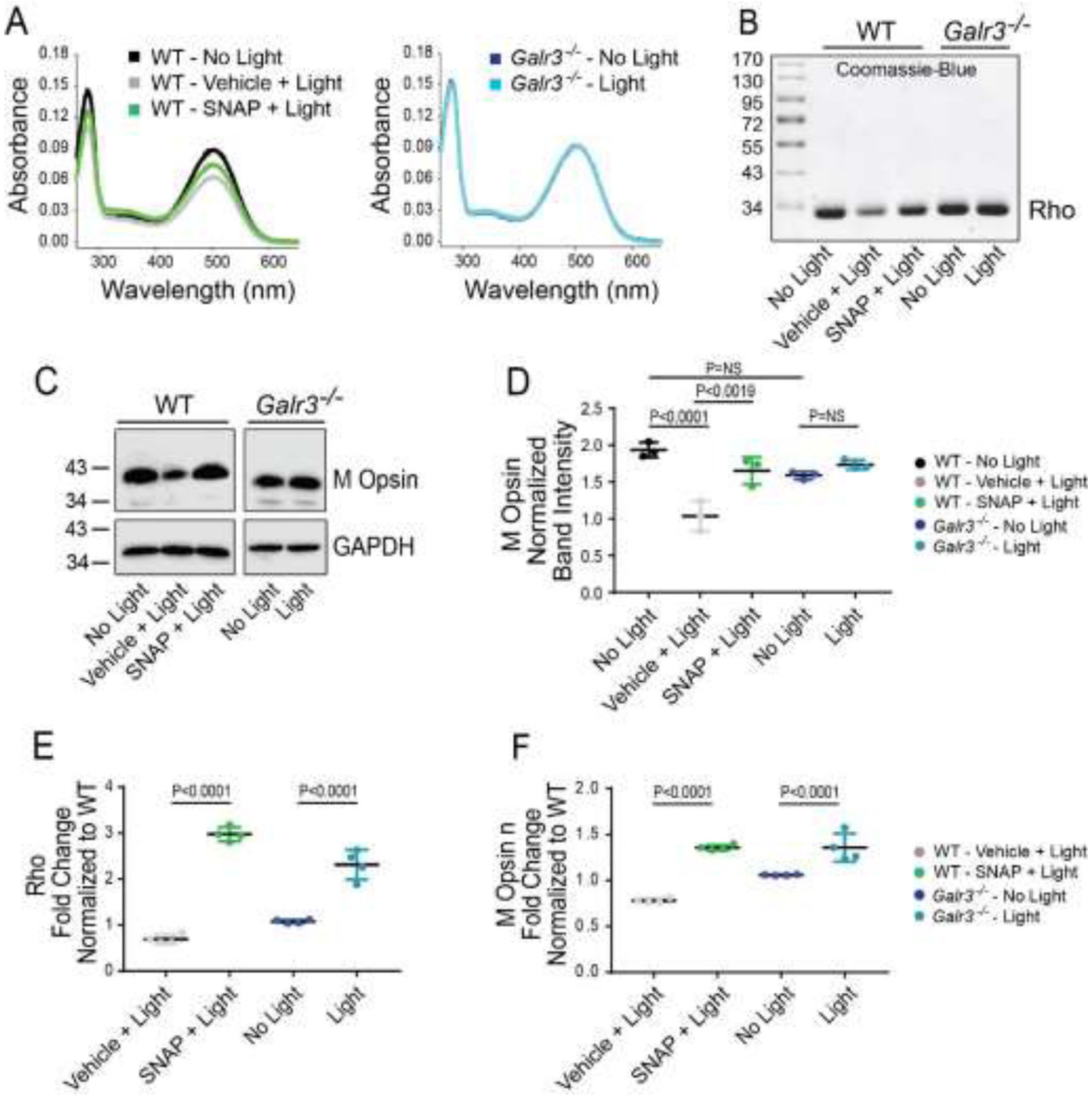

Figure 5. Inhibition of GALR3 allows maintaining levels of photoreceptor proteins Rho and M cone opsin in retinas injured with bright light.

A, UV-visible spectra of Rho purified from eyes (n = 6) of WT Balb/cJ mice dark-adapted, vehicle-treated and exposed to bright light, and treated with SNAP-37889 prior to illumination. In addition, Rho was purified from dark-adapted or exposed to bright light *Galr3*$^{-/-}$ mice on Balb/cJ background. **B**, The coomassie-blue-stained SDS-PAGE electrophoresis gel. The equal volumes of purified Rho fractions, shown in panel A, were loaded. The representative gel is shown. **C**, The representative immunoblots showing the

levels of M cone opsin in eyes of WT Balb/cJ mice either dark-adapted, vehicle-treated and exposed to bright light, or treated with SNAP-37889 prior to illumination, as well as dark-adapted or exposed to bright light *Galr3*$^{-/-}$-Balb/cJ mice. **D**, Quantification of M cone opsin expression. The intensity of M cone opsin expression was normalized to the expression of GAPDH. Error bars represent standard deviation (S.D.). **E-F**, The expression levels of Rho and M cone opsin determined by RT-qPCR. The relative fold of these genes expression was normalized to the expression of *Gapdh*. Error bars represent S.D. The *P* values for statistically different changes are indicated in the figure. Statistical analyses were performed with the two-way ANOVA and post hoc Turkey's tests. NS, not statistically significant.

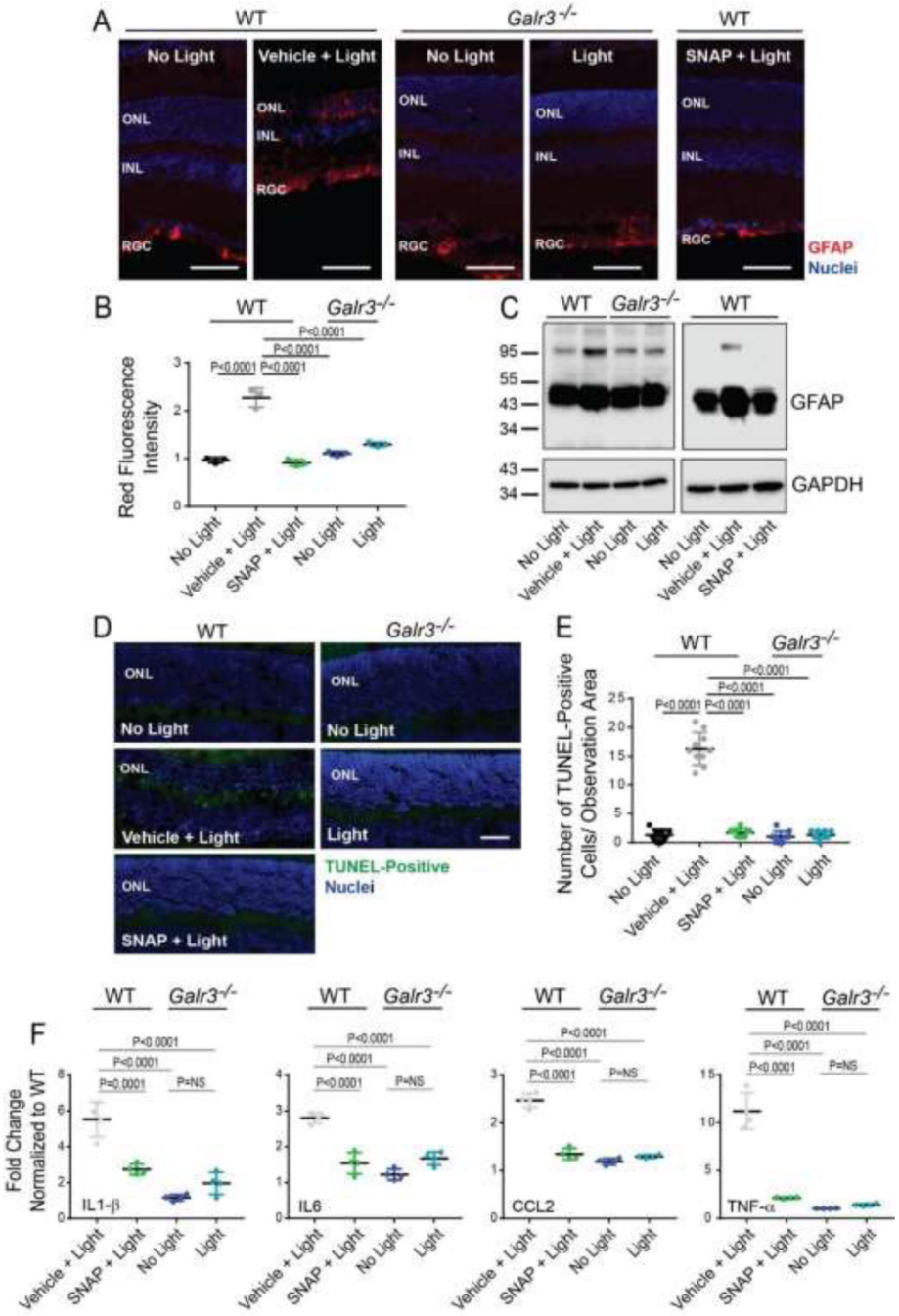

Figure 6. Inhibition of GALR3 is associated with downregulation of acute retinal inflammation.

A, Detection of GFAP on the retina cryosections prepared from eyes of dark-adapted, vehicle-treated and exposed to bright light, or SNAP-37889-treated prior to illumination WT Balb/cJ mice, and dark-adapted and exposed to bright light *Galr3*$^{-/-}$-Balb/cJ mice. Scale bar 50 μm. **B**, Quantification of GFAP expression as a mean of red fluorescence detected on the cryosections. Error bars represent standard deviation (S.D.). The *P* values for statistically different changes are indicated in the figure. **C**, The representative immunoblots showing the levels of GFAP in the protein extracts prepared from eyes of mice darkadapted, vehicle-

treated and exposed to bright light, or SNAP-37889-treated prior to illumination WT Balb/cJ mice, and dark-adapted or illuminated *Galr3*$^{-/-}$-Balb/cJ mice. **D**, TUNEL staining of the eye cryosections from WT Balb/cJ and *Galr3*$^{-/-}$-Balb/cJ mice. Green staining indicates dying photoreceptor cells. Blue indicates nuclei stained with DAPI. **E**, Quantification of TUNEL-positive photoreceptor cells. The *P* values for statistically different changes are indicated in the figure. Error bars represent S.D. **F**, The expression levels of proinflammatory markers IL1-β, IL6, and CCL2, and cell death marker TNF-α determined by RT-qPCR. The relative fold of these genes expression was normalized to the expression of *Gapdh*. The *P* values for statistically different changes are indicated in the figure. Statistical analyses were performed with the two-way ANOVA and post hoc Turkey's tests. NS, not statistically significant. ONL, outer nuclear layer; INL, inner nuclear layer; RGC, retinal ganglion cells.

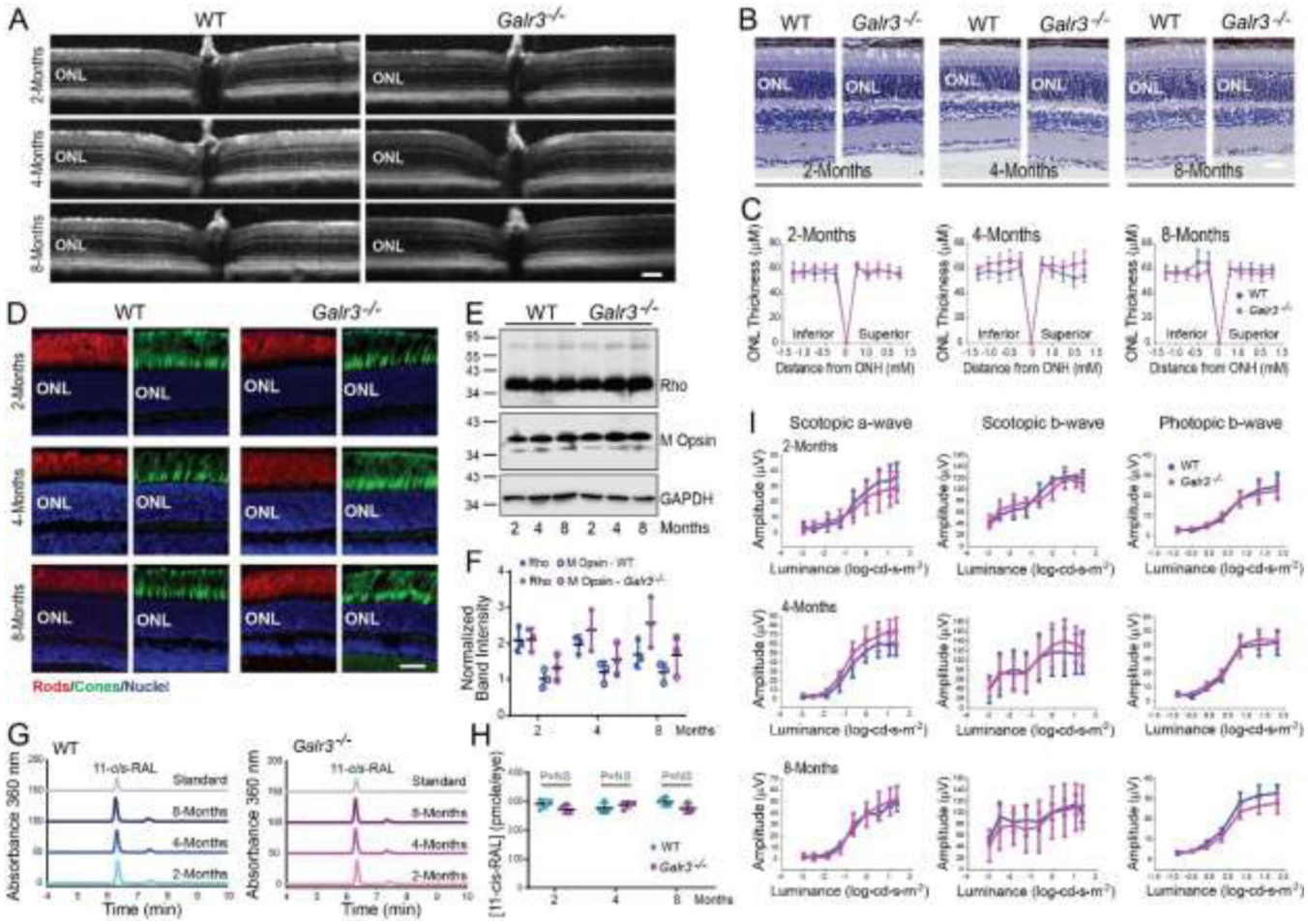

Figure 7. Ablation of the *Galr3* gene does not affect the overall retina health.

The health of the retina was examined in 2, 4, and 8-month-old *Galr3*$^{-/-}$ mice. Age littermates of C57BL/6J mice were used as WT control. **A,** The representative SD-OCT images of the retina. The B-scans shown here were taken at 0 degree. Scale bar 100 μm. **B**, The retina morphology was inspected in the hematoxylin and eosin (H&E)-stained paraffin eye sections. The images show the superior retina at ~0.5 mm from the optic nerve head (ONH). Scale bar 50 μm. **C**, The ONL thickness was measured at 0.25, 0.5, 0.75, 1.0, and 1.25 mm from the ONH. The measurement was performed in n = 6 mice per group. No statistical differences were found between *Galr3*$^{-/-}$ and WT mice. Error bars represent standard deviation (S.D.). **D**, The representative retinal cryosections stained with anti-Rho antibody to detect rod photoreceptors and peanut agglutinin (PNA) to detect cone photoreceptors. The images show the superior retina at ~0.5 mm from the ONH. Nuclei were stained with DAPI. Scale bar 25 μm. **E and F**, Immunoblots examining the levels of Rho and M opsin at 2, 4, and 8 months of age in *Galr3*$^{-/-}$ and WT mice and their quantification, respectively. The representative immunoblots are shown. The band intensities were normalized to the intensities of GAPDH. Error bars represent S.D. **G and H**, Retinoid analysis at 2, 4, and 8 months of age in *Galr3*$^{-/-}$ and WT mice and quantification of the 11-*cis*-retinal oximes, respectively. The elution profiles of retinoid oximes extracted from mouse eyes are shown in G. The concentration of the 11-*cis*-retinal oximes per eye in each

experimental group is shown in H. Error bars represent S.D. No statistical differences in the 11-*cis*-retinal oximes concentration were found between *Galr3*$^{-/-}$ and WT mice. **I**, Retinal function was examined by measuring the electroretinography (ERG) responses. Both a-wave and b-wave responses were measured in n = 5 mice per group. No statistical differences in the ERG responses were found between *Galr3*$^{-/-}$ and WT mice. Error bars represent S.D. Statistical analyses were performed with the two-way ANOVA and post hoc Turkey's tests. NS, not statistically significant. ONL, outer nuclear layer.

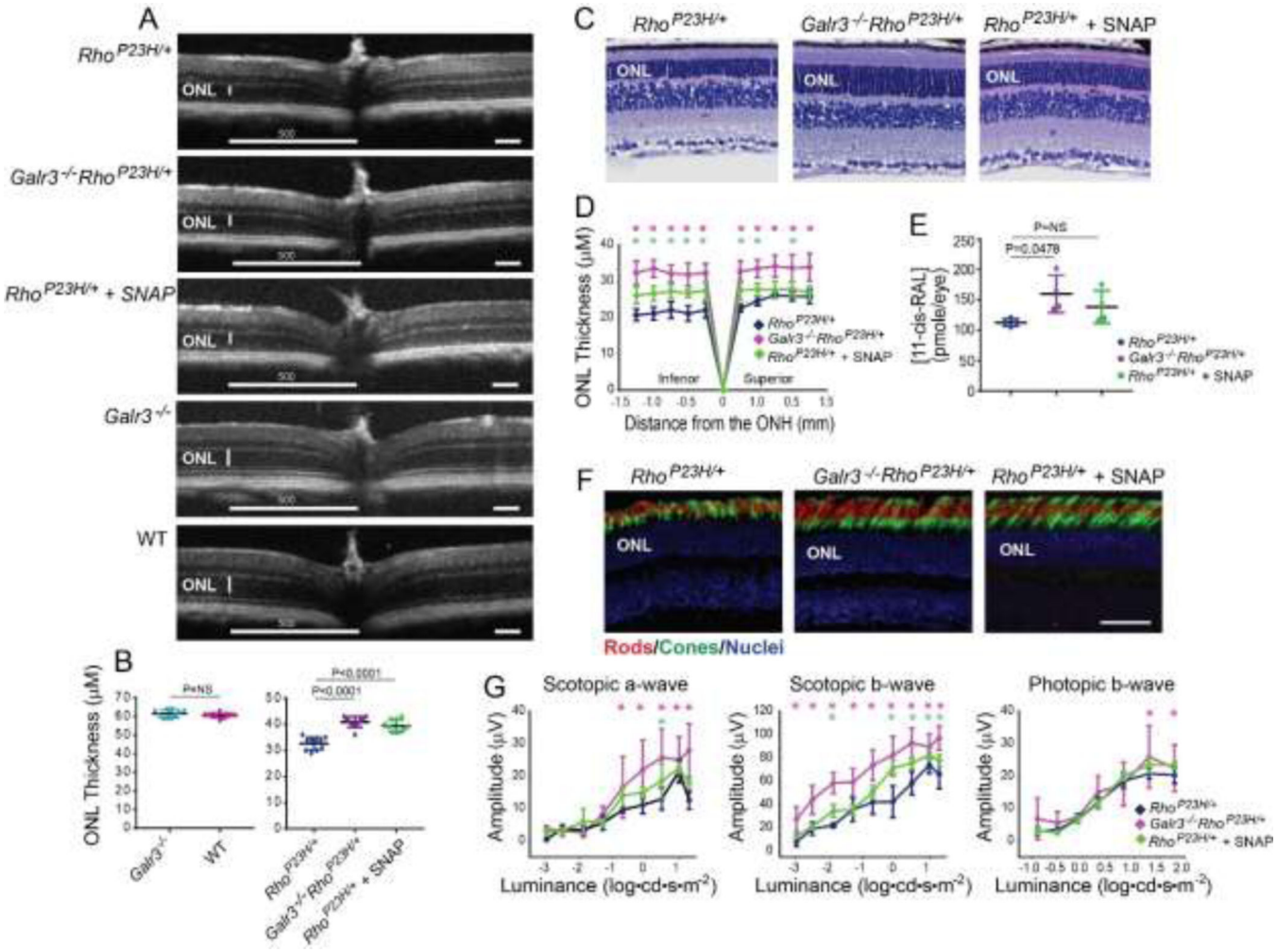

Figure 8. Ablation of *Galr3* or pharmacological inhibition slows down retina degeneration in Rho-related retinitis pigmentosa.

Galr3$^{-/-}$ were cross-bred with *Rho*$^{P23H/P23H}$ to generate *Galr3*$^{-/-}$*Rho*$^{P23H/+}$ mice to evaluate if inhibition of GALR3 could have a protective effect in chronic retinopathy. In addition, *Rho*$^{P23H/+}$mice were treated with SNAP-37889 every other day from P21 to P33. **A**, A comparison of the representative SD-OCT images of the retina of *Rho*$^{P23H/+}$, *Galr3*$^{-/-}$*Rho*$^{P23H/+}$, *Rho*$^{P23H/+}$-treated with SNAP-37889, and *Galr3*$^{-/-}$ mice at P33. Scale bar 100 μm. **B**, The measurement of the ONL thickness at 500 μm from the optic nerve head (ONH) in the SD-OCT images. The measurement was performed in n = 6 mice per group. Error bars represent standard deviation (S.D.). The *P* values for statistically different changes are indicated in the figure. **C**, The retina morphology of *Rho*$^{P23H/+}$, *Galr3*$^{-/-}$*Rho*$^{P23H/+}$, and *Rho*$^{P23H/+}$ mice treated with SNAP-37889 inspected in the hematoxylin and eosin (H&E)-stained paraffin eye sections. Scale bar 50 μm. **D**, The retina and the ONL thickness were measured at 0.25, 0.5, 0.75, 1.0, and 1.25 mm from the optic nerve head (ONH). The measurement was performed in n = 6 mice per group. Error bars represent S.D. **E**, Retinoid analysis. The concentration of the 11-*cis*-retinal oximes per eye in each experimental group (n = 5 mice per group) is shown. Error bars represent S.D. The *P* values for statistically different changes are indicated in the figure. **F**, The representative

retinal cryosections stained with anti-Rho antibody to detect rod photoreceptors and peanut agglutinin (PNA) to detect cone photoreceptors in $Rho^{P23H/+}$, $Galr3^{-/-}Rho^{P23H/+}$, and $Rho^{P23H/+}$ mice treated with SNAP-37889. Nuclei were stained with DAPI. Scale bar 25 μm. **G**, Retinal function was compared in $Rho^{P23H/+}$, $Galr3^{-/-}Rho^{P23H/+}$, and $Rho^{P23H/+}$ treated with SNAP-37889 mice at P33. The electroretinography (ERG) responses were measured in n = 5 mice per group. Inhibition of GALR3 substantially protected both a-wave and b-wave responses in $Galr3^{-/-}Rho^{P23H/+}$ mice as compared to $Rho^{P23H/+}$ mice. Error bars indicate S.D. Statistically different changes ($P < 0.05$) are indicated with asterisks. Statistical analyses were performed with the two-way ANOVA and post hoc Turkey's tests. NS, not statistically significant.

Table 1.

List of used commercial antibodies.

Antibody Name	Species	Source	Identifiers	Additional information
Anti-GALR1	Rabbit polyclonal	LSBio	LS-C120666	1:1000
Anti-GALR2	Rabbit polyclonal	LSBio	LS-C805729	1:1000
Anti-GALR3	Rabbit polyclonal	Thermofisher	PA5-19206	1:200
Anti-GFAP	Rabbit polyclonal	Thermofisher	PA1-9565	1:1000
Anti-GAPDH	Mouse monoclonal	Abclonal	AC002	1:10,000
Anti-mouse IgG, HRP conjugate	Goat	Promega	W4021	1:10,000
Anti-rabbit IgG, HRP conjugated	Goat	Promega	W4011	1:10,000
Anti-mouse IgG Alexa Fluor 555-conjugated	Goat	Thermofisher	A28180	1:400
Anti-rabbit IgG Alexa Fluor 555-conjugated	Goat	Thermofisher	A27039	1:400
Anti-mouse IgG Alexa Fluor 488-conjugated	Goat	Thermofisher	A28175	1:400

Table 2.

List of used primers.

Target	Species	Forward primer sequence 3'→5'	Reverse primer sequence 3'→5'
Rhodopsin	mouse	CTTCCTGATCTGCTGGCTTC	ACAGTCTCTGGCCAGGCTTA
mOpsin	mouse	GAGATTCAAGAAGCTGCGCC	TGTCCAGAACGAGTAGCC
Gapdh	mouse	TTGAGGTCAATGAAGGGGTC	TCGTCCCGTAGACAAAATGG
TNF-α	mouse	GGTCTGGGCCATAGAACTGA	CAGCCTCTTCTCATTCCTGC
IL1-β	mouse	TGCCACCTTTTGACAGTGATG	AAGGTCCACGGGAAAGACAC
IL6	mouse	CAACGATGATGCACTTGCAGA	GTGACTCCAGCTTATCTCTTGGT
CCL2	mouse	TCTCCAGCCTACTCATTGGG	AGGTCCTGTCATGCTTCTG
Spexin	mouse	CGCCTCCAGAAAGACGAAAC	AATTCCCTCCTTCATCTGCACC
Galr3	mouse	TCGTGTGCAAGACGGTACA	ACCGCCAGGTACCTATCCA